Investigating the link between aerobic respiration and antimicrobial susceptibility in pathogenic *Escherichia coli*

Thesis for MSc by Research in Microbiology

School of Biosciences

University of Kent

Safura Fusseini

2020

Declaration

I confirm that no part of this thesis has been submitted in support of an application for any degree or other qualification of the University of Kent, or any other University or Institution of learning.

Safura Fusseini

16th December 2020

Abstract

There has been a significant emergence of antimicrobial resistance in bacterial pathogens, so understanding factors that modulate the efficacy of antibiotics is therefore crucial. Studies have previously reported a relationship between aerobic respiration and bactericidal antibiotics, where the inhibition of aerobic respiration protects bacterial cells from the lethal effects of antibiotics. However, the loss of respiratory oxidase activity will both decrease the proton motive force (PMF) and diminish the oxygen chemistry. Given that the PMF is used for the entry of positively-charged antibiotics into the bacterial cell, two explanations exist to explain why aerobic respiration promotes antibiotic killing: i) reactive oxygen species are produced, ii) the PMF resulting from respiratory activity promotes antibiotic uptake. During infection, the respiratory inhibitor nitric oxide (NO) is released from the immune system which could clearly impact upon the efficacy of antibiotics. Hence, it was of interest to investigate how NO might affect the efficacy of antibiotics against bacterial pathogens.

Previous work in the Shepherd lab has reported that NO diminishes the efficacy of the positively charged antibiotic gentamicin against *E. coli*, so the impact of NO upon the PMF was investigated using the PMF-sensitive dye ($DISC_3(5)$). The data obtained clearly show that NO decreases the PMF, suggesting that antibiotic uptake (and toxicity) could be diminished by a NO-mediated decrease in the PMF. To further investigate this, the effects of NO upon the positively charged antibiotic nitrofurantoin were investigated with *E. coli*. These data show that rather than decreasing toxicity, NO increased the toxicity of nitrofurantoin. Subsequent work with mutant strains that express single respiratory oxidases with varying sensitivities to NO suggest that inhibition of the final step of aerobic respiration may be linked to a build-up of electrons in the quinol pool resulting in more effective activation of nitrofurantoin in the cytoplasm, although further work will be needed to confirm this.

This work describes a novel synergistic relationship between NO and nitrofurantoin-mediate bacterial killing, which is particularly relevant for the treatment of UTIs. This enhances our understanding of why nitrofurans are effective antimicrobials and may impact upon future approaches to treat UTIs produced by antibiotic-resistant Gram-negative bacteria.

Acknowledgements

Firstly, I would like to show gratitude to my supervisor Dr Mark Shepherd for the countless guidance, assistance and mentorship during this year, which has been considerably challenging. I am very grateful for the chance to complete this research and add to the work performed in your lab as well as developing my scientific skill, which would be beneficial to me in the foreseeable future. Also, I would like to acknowledge the members of the Shepherd's and Robinson's lab (Louis, Calum and Sarah) as well as Dr Gary Robinson for all the assistance in guiding me through the lab protocols, method development and training.

I am very grateful for all the post-graduate students I developed a friendship with. Thank you for all the support and endless advice, especially in times when I was stressed and had doubts about the process.

Lastly, to my parents and close friends. I would like to thank them for the endless support and encouragement throughout this process especially during the last few months. They have always been there for me, giving me that push when I am in doubt and that determination to excel in everything I do. And Mohammed, for all the love and support you have given me, inspiring me to do better, and for encouraging me to believe in myself.

Abbreviations

Acriflavine - ACR

Adenosine Triphosphate - ATP

Antimicrobial resistance – AMR

Chloramphenicol – Cm

Chloramphenicol resistance - Cm^R

Electron transport chain – ETC

Gentamicin - Gm

Methicillin- resistant *staphylococcus* aureus – MRSA

Multidrug resistant – MDR

Nitric oxide – NO

Nitrofurantoin - NF

Proton motive force - PMF

Reactive oxygen species – ROS

S- Nitrosoglutathione - GSNO

Transmembrane domain – TMD

Tricarboxylic acid cycle – TCA

Urinary tract infections - UTI

Table of Contents

List of figures

List of Tables

Chapter 1

Introduction

1.1 Antimicrobial resistance (AMR)

1.1.1 Overview of antibiotic resistance crisis

Antibiotics are the main drug used in clinical medicine to fight infections. There was a boom in antibiotic discovery from the 1930s up until the 1960s, after which researchers saw a significant emergence of resistant pathogens (Singer *et al*. 2016). Pathogens known as 'Eskape pathogen' are one of the leading causes of multidrug-resistance (MDR). This includes bacteria that are both gram positive and negative such as *Enterobacter* species (Mulani, Kamble, Kumkar, Tawre and Pardesi 2019). Bacteria in this group cause nosocomial infection with significant resistance due to different drug resistant mechanisms (Mulani, Kamble, Kumkar, Tawre and Pardesi 2019). Antibiotic resistance has led to serious impact on animals, humans as well as the environment (Singer *et al.* 2016). This is caused by the emergence and spread of MDR bacteria (Marshall and Levy 2011; Micheal, Dominey-Howes and Labbate 2014). The cause of this resistance includes factors such as antibiotics in animals and humans consistently being used, an increase in travel internationally, poor hygiene, and the release of antibiotics that are non metabolized (Aslam *et al*. 2018). Factors including horizontal gene transfer and spontaneous mutations lead to the spread of MDR bacteria (Figure 1.3). These factors influence genetic selection pressures for the rise in MDR bacterial infections, therefore making it harder for antibiotics to be effective (Aslam *et al*. 2018; Figure 1.3). Recent analyses of bacterial genomes have revealed that there are more than 20,000 potential resistance genes (Aslam *et al.* 2018), and the World Health Organisation announced antibiotic resistance to be a 'global public health concern' (Micheal, Dominey-Howes and Labbate 2014; Spellberg, Srinivasan and Chambers 2016).

Antibiotic resistance shows no indications of declining and continues to be a major global economic liability. In the USA, 99,000 deaths are caused annually by antibiotic-resistant pathogen-associated hospital acquired infection (HAIs) (Guidos 2011). This also leads to additional days in the hospital causing extra money lost (Guidos 2011). Thus, we need a greater understanding of this crisis. Therefore, to create new therapeutics researchers need to understand the methods that bacteria use to escape the toxicity of current antibiotics.

1.1.2 The emergence of antibiotic resistance

The breakthrough of penicillin made from fungus in 1928 led to the modern era of antimicrobial chemotherapy. During World War II, the drug of preference was penicillin which was used to manage infections caused by bacteria (Sengupta, Chattopadhyay and Grossart 2013; Piddock 2012). The use of penicillin decreased the number of deaths and amputations during World War II (Sengupta, Chattopadhyay and Grossart 2013). Following widespread use, resistance to penicillin emerged. Scientists then developed a novel β-lactam antibiotic to combat this (Aslam *et al.* 2018). The core structure of penicillin is composed of a β-lactam ring, which are quite reactive such as carbapenems, cephalosporins, monobactams, beta-lactamase inhibitors (Pandey and Cascella 2020). Peptidoglycans is a polymer consisting of alternating crosslinked chains of N-acetyl muramic acid (NAM) and N-acetylglucosamine (NAG) by four amino acids. This is an important element of the bacterial cell wall which provides mechanical stability. Penicillin works by inhibiting the last step in the synthesis of peptidoglycans by acylating the transpeptidase involved in crosslinking peptides to form the polymer (Pandey and Cascella 2020). As penicillin is similar to the D-alanyl-D alanine portion found in NAM, the enzyme required for the transpeptidation reaction reacts with the β-lactam nucleus, leading to its inactivation (Soares, Figueiredo, Faveri, Cortelli, Duarte and Feres 2012). Thus, the peptidoglycan chain that forms has weak points due to no crosslinks being formed. This leads to osmotic lysis caused by cell rupture (Soares, Figueiredo, Faveri, Cortelli, Duarte and Feres 2012). Other targets for penicillin are called penicillin-binding proteins (Soares, Figueiredo, Faveri, Cortelli, Duarte and Feres 2012; Pandey and Cascella 2020). Another notable case of resistance occurred in methicillin-resistant *Staphylococcus aureus* (MRSA), which was first reported in the 1960s (Sengupta *et al.* 2013; Spellberg and Gilbert 2014). Vancomycin was used to treat MRSA. Soon after, coagulase-negative vancomycin resistance was reported (Sengupta *et al.* 2013). MRSA infections are most common in hospital settings but have now become much more frequent in the community as well (Arede *et al.* 2012). Further evidence of clinically relevant antimicrobial-resistance in bacterial pathogens is seen for *Clostridium difficile*. The bacterial pathogen, *C. difficile* infects the bowel and can lead to diarrhoea (Bamberg *et al*. 2015). This occurs by the exposure of normal intestinal microbiota to antibiotics that are inactive against *C. difficile*, leading to flora disruption and the spread of *C. difficle* (Hirota and Sun 2015). As *C. difficile* is a spore-forming organism, the spores can endure antimicrobial treatment and germinate, causing the recurrence of infection (Hirota and Sun 2015). The use of antibiotics is a possible risk issue (Lamont and Leffler 2015), making treatment quite difficult due to

resistance of various antibiotics such as aminoglycosides, tetracyclines, fluoroquinolones and many other common chemical classes, which are commonly used in clinical settings. In addition, fluoroquinolones are also known to promote the infection (Lamont and Leffler 2015). The elimination of normal flora in the gastrointestinal tract allows toxic strains of *C. difficile* to proliferate (Lamont and Leffler 2015). To date, *C. difficile* causes ~453,000 cases and ~29,000 deaths annually in the USA and is one of many urgent threats caused by AMR (Bamberg *et al.* 2015).

More recently, multidrug-resistant Gram-negative bacterial strains such as Eskape pathogens are emerging as a major threat to human health. A well-characterised example is *Escherichia coli* ST131, a globally circulated sequence type that is resistant to various classes of antibiotics (Totsika *et al.* 2011). *E. coli* ST131 produces extended-spectrum β-lactamases such as CTX-M-15, protecting it from the effects of β-lactam antibiotics (Laupland and Pitout 2008). *E. coli* ST131 isolates are highly pathogenic due to the carriage of many virulence-associated genes. Some strains cause diarrheal illness, while others cause extraintestinal infections (Laupland and Pitout 2008). However, this is one of many causes of urinary tract infections (Laupland and Pitout 2008). Strains of *E.coli* ST131 are associated with serotype O25 (molecular subtype):H4 and belong to the phylogenetic group B2 (Blanco 2008). *E. coli* EC958 is one example of a *E. coli* ST131 strain that is used in the current study (Blanco 2008; Forde *et al*. 2014; Laupland and Pitout 2008; Totsika *et al*. 2011). This is one of the most characterised strains of *E. coli* ST131, which was taken from a urine sample isolated from an 8-year-old girl in March 2005 in the United Kingdom (Forde *et al*. 2014). It is a fluoroquinolone resistant strain consisting of multiple genes linked to the virulence of extra-intestinal *E. coli* (Forde *et al*. 2014). This includes genes encoding for siderophores, adhesins and autotransporter protein receptors (Forde *et al*. 2014). It expresses type 1 fimbriae which is needed for the invasion and adherence of human bladder cells (Forde *et al*. 2014).

1.2 Classes of antimicrobial agents

Most antimicrobial agents are generated by microbes such as environmental fungi or saprophytic bacteria, while others may be altered variants of natural compounds or are chemically synthesised such as fluoroquinolones and sulphonamides (Holmes *et al.* 2016). Antibiotics are classified either by its chemical structure, mode of action or phenotypic effect on the microorganism (Table 1.1). Aminoglycosides, amphenicols and nitrofurantoin

are described in detail further below as they were the main antibacterial agents used in this study.

1.2.1 Aminoglycosides

Aminoglycosides are bactericidal antibiotics that consist of amino sugars that are bonded by a glycosidic linkage to a dibasic aminocyclitol (Mingeot-Leclerceq *et al.* 1999). They are classified depending on the identity of the aminocyclitol moiety (Magnet and Blanchard 2005; Wachino and Arakawa 2012). These were first discovered from the isolation of *Streptomyces griseus* in 1944 (Wachino and Arakawa 2012). Over a few decades, other antibiotics classified in this group were discovered and then second-generation semi-synthetic versions were made. Examples of common aminoglycosides include: neomycins, gentamicin and kanamycin (Wachino and Arakawa 2012). Gentamicin was used during this study, it consists of a 4,6- di-substituted deoxystreptamine ring, which is an aminocyclitol moiety (Figure 1.1)

The aminoglycoside antibiotics act by binding to 16s rRNA that are part of the 30s subunit and interrupting protein synthesis, thus leading to cell death (Wachino and Arakawa 2012). This in turn leads to translational errors by inhibiting translocation. Many bacteria have developed resistance to this by methylation or substitution of the bases that bind to 16s rRNA. This leads to the mutation of the target binding site. Also, reduces the uptake of the drug through changes to the membrane permeability and efflux (Courvalin, Galimand and Lambert 2003).

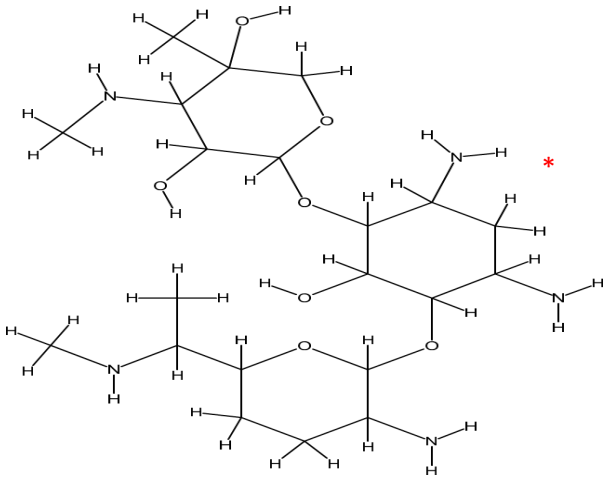

Figure 1.1 Chemical structure of gentamicin. The asterisk represents the 4,6 di-substituted deoxystreptamine ring, which is bonded together by glycosidic bonds to amino sugars.

Table 1.1 Common antibiotics classes and mode of action (Brunning 2014).

Antibiotic classes	Mode of action	Common resistance mechanism
β- lactam	Inhibit bacterial cell wall synthesis by binding to substrate-anchoring site where D- alanyl-D- alanine is occupied (Tipper and Strominger1965).	Hydrolysis of β-lactam ring (Tipper and Strominger 1965)
Aminoglycosides e.g., gentamicin	Inhibit protein synthesis by binding to rRNA leading to cell death (Wachino and Arakawa 2012; Fourmy, Recht, Blanchard and Puglisi 1996).	Modification of antibiotic structurally by mutation of ribosomal protein (Wachino and Arakawa 2012)
Amphenicols (Chloramphenicol)	Inhibits synthesis of protein by binding to 50s ribosomal unit on peptidyl transferase (Allison *et al*. 1962)	Enzymatic inactivation by drug acetylation via chloramphenicol acetyltransferases (Murray and Shaw 1997)
Tetracyclines	Binds to subunit of ribosomes, inhibiting protein synthesis	ribosomal protection from antibiotic and efflux pumps
Macrolides	Binds to subunit of ribosomes, inhibiting protein synthesis (Leclercq 2002)	Blockage of ribosomal binding, drug inactivation, efflux pump (Leclercq 2002)
Quinolones	Conversion of topoisomerase IV and gyrase into toxic enzymes. Degradation of DNA	Alteration of antibiotics and efflux pumps

1.2.2 Amphenicols (chloramphenicol)

In the late 1940s, it was isolated from *Streptomyces venezuelae,* as an antibiotic and from then on it has been chemically synthesised (Allison *et al.* 1962). Chloramphenicol is bacteriostatic and causes the inhibition of protein synthesis via binding irreversibly to the 50s ribosomal subunit (Allison *et al.* 1962; Xaplanteri *et al.* 2003). Resistance can occur by inactivating its effects through acetyltransferases (Schwarz *et al*. 2004).

1.2.3 Nitrofurantoin

Nitrofurantoin is a bactericidal antibiotic drug, which has been available since the 1950s (Figure 1.2). It is commonly used to treat different types of UTIs such as those caused by *E. coli* EC958 (Gardiner *et al*. 2019). The mode of action has not been understood yet, but it has been said to be multifactorial (Gardiner *et al*. 2019). However, what is known is that it produces extremely reactive electrophilic metabolites by reducing bacterial enzymes (Gardiner *et al.* 2019). Thus, inhibiting protein synthesis from obstructing bacterial ribosomal proteins (Blass 2015). Within *E. coli* it utilises NADH and nitro reductase to form nitroaryl anion free radicals, reactive oxygen species (ROS) like many bactericidal antibiotics (Blass 2015). Thus, damaging vital components in bacteria such as DNA, leading to cell death.

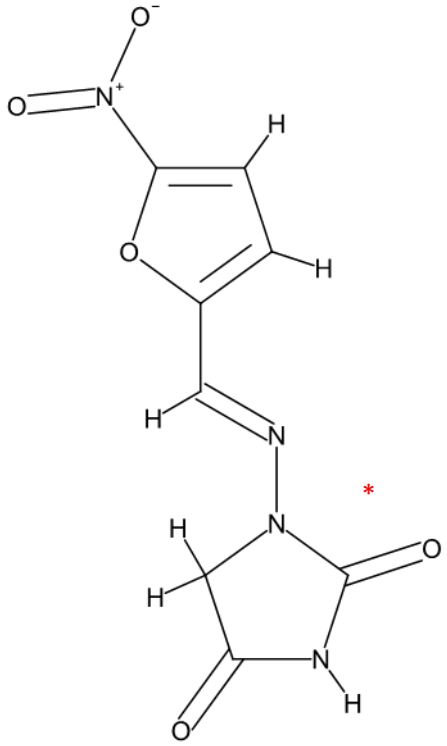

Figure 1.2 Chemical structure of nitrofurantoin. It consists of a hydantoin ring, this is represented by the asterisk with nitro-substituted furanyl side chain. When inside the bacteria its metabolised to produce reactive compounds.

1.3 Mechanisms leading to antimicrobial resistance

Most organisms evolve defensive mechanisms against antibiotics such as alteration of target site, drug entry or distribution inhibition and production of enzymes that can result in the degrading of the antibiotic, thus making it less effective resulting in resistance

(Forsberg *et al.* 2016; Aminov 2009; Figure 1.3; Table 1.1). The consistent use of antibiotics is the main reason of resistance, also warned by Sir Alexander Fleming 'public will demand the drug, and this will begin an era of abuse' (Aslam *et al*. 2018). Sensitive bacteria can be eradicated by antibiotics, but resistant pathogens can linger, these reproduce thus survive by natural selection (Aslam *et al.*2018) and horizontal gene transfer.

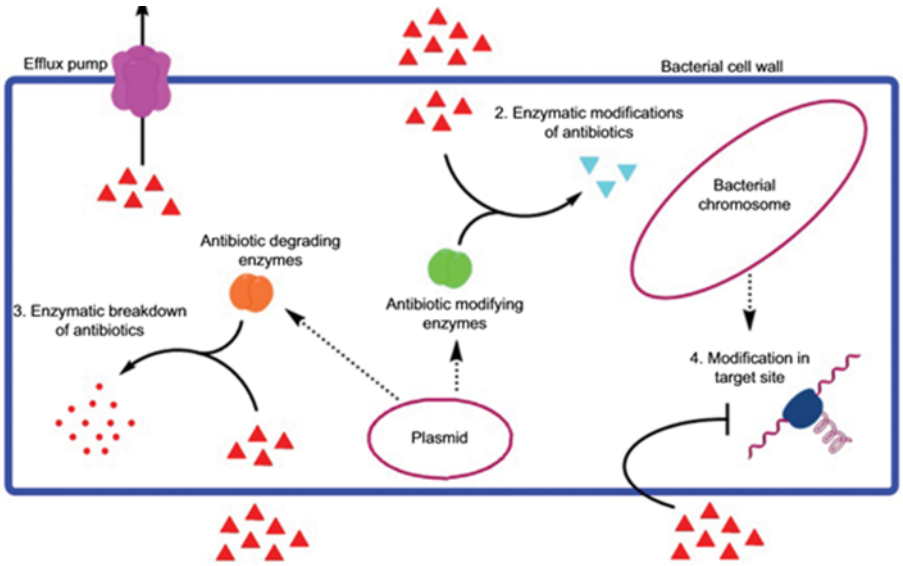

Figure 1.3 The portrayal of various mechanisms bacteria acquires which allows it to be resistant to antibiotics (Aslam *et al.* 2018).

1.3.1 Horizontal gene transfer

Horizontal gene transfer is the transfer of genetic information between genomes (Choudhuri 2014). It includes the gene transfer within species boundaries, allowing them to share genes (Choudhuri 2014). In bacteria, three important mechanisms facilitate gene transfer: transformation (uptake of free DNA), conjugation (transfer of plasmid) and transduction (phage-mediated transfer) (Choudhuri 2014). Transformation is most frequent in bacteria that can transform naturally (Kevorkov, Legendre and Makarenkov 2016). Naked DNA fragments from the environment are taken up (Kevorkov, Legendre and Makarenkov 2016). This gene transfer allows the exchange of any part of a chromosome (Kevorkov, Legendre and Makarenkov 2016). Conjugation is mediated by conjugal transposons or plasmids (Kevorkov, Legendre and Makarenkov 2016). The process of conjugation usually occurs between distant related bacteria or between bacteria and eukaryotes but usually requires cell to cell contact (Kevorkov, Legendre and Makarenkov 2016). The process of transduction allows DNA to be transferred by bacteriophages

(Kevorkov, Legendre and Makarenkov 2016). Cell surface receptors are shared for phage binding between the donor and receptor (Kevorkov, Legendre and Makarenkov 2016). However, transduction occurs between closely related bacteria (Kevorkov, Legendre and Makarenkov 2016). Whereas transformation and conjugation is the opposite (Kevorkov, Legendre and Makarenkov 2016). Horizontal gene transfer enables resistance to spread quickly through species. This is another problem which makes combating antibiotic resistance harder.

1.4 Respiration influences antibiotic susceptibility

1.4.1 Bacterial respiration impacts antimicrobial susceptibility

While antibiotics have different primary modes of action, one common feature is that the respiratory chain can have a major impact upon the lethality of a range of different antibiotics. Indeed, different studies have shown there to be a link between antibiotic treatment and respiration (Lobritz *et al*. 2015; Kohanski *et al.* 2007). Bacteriostatic antibiotics suppress cellular respiration thus causing growth inhibition (Lobritz *et al*. 2015; Kohanski *et al.* 2007). However, bactericidal antibiotics elevate respiration by exacerbating its toxic effect leading to cell death (Lobritz *et al*. 2015). In this study, respiratory knockouts were shown to demonstrate that diminished aerobic respiration resulted in a decrease in antibiotic lethality. To accelerate respiration, ATP synthesis was uncoupled from the electron transport chain (ETC), increasing the lethality of bactericidal drugs (Lobritz *et al.* 2015). ROS have been shown to be very important in initiating cell death in bactericidal drugs. The basic mechanism of cell death is seen in Figure 1.4. When bacteria are treated with bactericidal antibiotics, hydroxyl radicals are produced through oxidative damage in a cellular death pathway. By changes to the tricarboxylic acid cycle (TCA) and iron metabolism (Kohanski *et al*. 2007; Kohanski, Dwyer and Collins 2010).

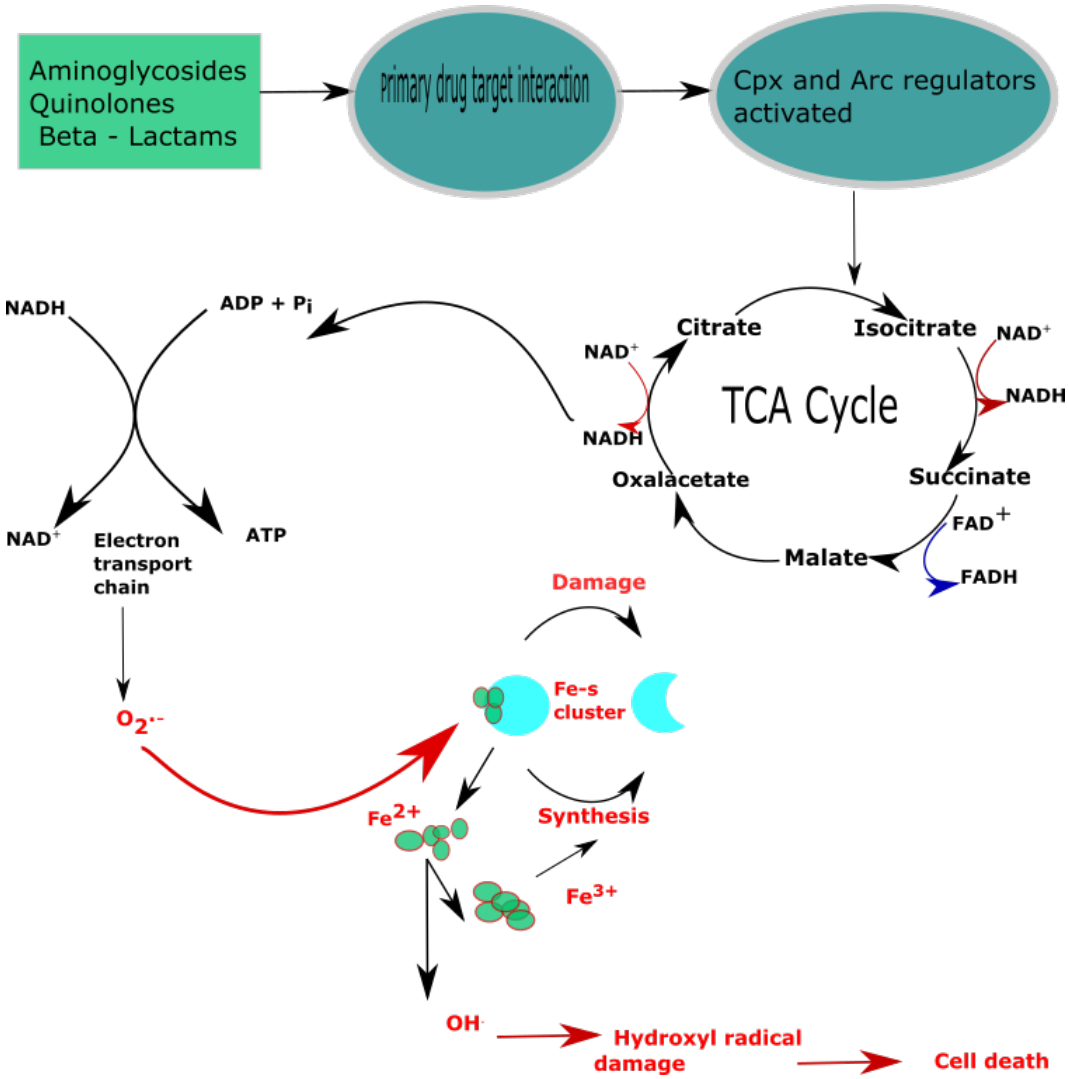

Figure 1.4 The proposed model for the mechanism of bactericidal killing from the creation of ROS. This involves the creation of ROS via hyperactivation of the ETC leading to cell death. This is believed to be the main factor contributing to cell death by antibiotics.

Bactericidal antibiotics (β-lactam, quinolones, and aminoglycosides) enters the bacterial cell and interact with their targets (Kohanski, Dwyer and Collins 2010; Figure 1.4). The TCA cycle is stimulated by Cpx and Arc regulators in response to cellular stress (Kohanski, Dwyer and Collins 2010; Kohanski *et al*. 2007), which elevates NADH production and respiratory activity. The hyperactivation of the ETC stimulates the formation of ROS including hydrogen peroxide and superoxide (Imlay *et al.* 2003; Kohanski *et al.* 2007). In addition, to the build-up of superoxide that destabilises iron-sulfur clusters, which releases ferrous iron that can participate in Fenton chemistry (Kohanski *et al*. 2007). Hydroxyl radicals are formed from the Fenton reaction, which severely damages proteins, DNA and

lipids resulting in cell death (Kohanski *et al* 2007; Kohanski, Dwyer and Collins 2010). While ROS generation does appear to be a common theme for most antibiotics, for positively charged aminoglycosides an alternative mechanism has been proposed to explain the relationship between antibiotic toxicity and respiratory activity: a rapid increase in ETC activity results in a large PMF, which can promote aminoglycoside entry into the cytoplasm (Ezraty *et al.* 2013).

1.4.2 The aerobic respiratory chain of *E. coli*

Given the importance of aerobic respiration in antibiotic toxicity, and the experimental approaches used in the current study, it is important to introduce the aerobic respiratory chain of *E. coli*. The respiratory system of bacteria consists of branched respiratory chains, where different components are expressed under different conditions (Borisov *et al.* 2011). *E. coli,* a facultative anaerobic pathogen, can live in aerated and anoxic conditions as well as possessing an adaptable respiratory chain that allows it to survive in either environment.

Aerobic respiration involves using the ETC by moving electrons from an electron donor, such as NADH, to a terminal electron acceptor such as oxygen. The movement of electrons along the respiratory chain releases energy, which is conserved as a proton motive force (PMF) throughout the inner membrane. Thus, the PMF is used for processes such as ATP synthesis. Three terminal oxidase complexes are present in *E. coli* that catalyse the reduction of oxygen, also has an effect on the PMF (Sousa *et al.* 2012). This would be discussed below in further detail.

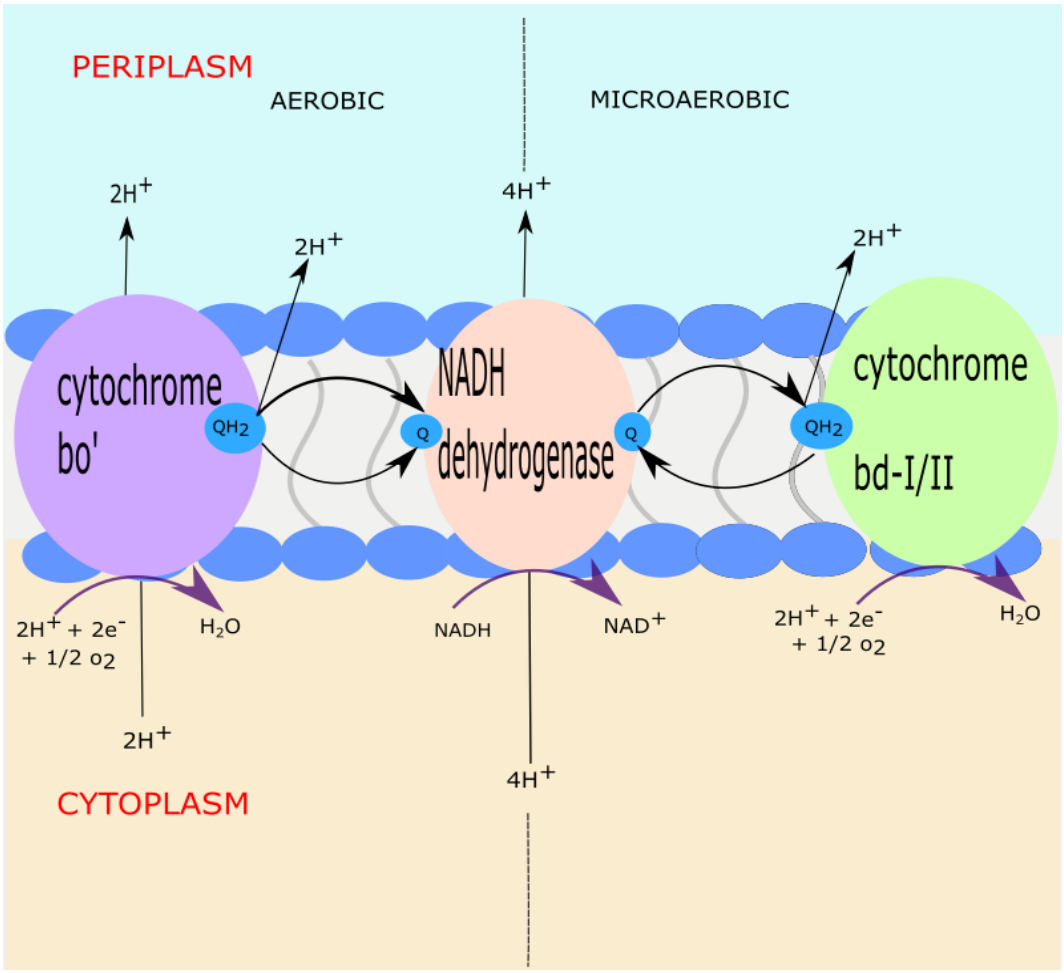

Figure 1.5 Elements present in aerobic respiratory chain of *E. coli*. In low oxygen conditions two types of cytochrome *bd* are expressed: *bd-I* and *bd-II*. *bd-II* is upregulated under starvation/phosphate stress and in aerobic conditions cytochrome *bo'* is expressed.

E.coli aerobic respiration requires three respiratory complex that generate a PMF: I) a proton-pumping NADH quinone oxidoreductase NADH dehydrogenase I (NDH-1); ii) cytochrome *bo'* quinol oxidase, a proton-pumping oxygen reductase which is part of the superfamily of haem-copper oxidoreductase; and iii) *bd*-type cytochrome quinol oxidases, which cannot pump protons but generates a PMF via vectoral proton translocation linked to quinol oxidation (Borisov *et al*. 2011; Figure 1.5; Puustinen *et al*. 1991). Cytochrome *bo'* is a haem-copper oxidase and is expressed when the oxygen level is more than 20% (Tseng, Albrecht and Gunsalus 1996). Cytochromes *bd*-I is expressed in microaerobic conditions (Borisov *et al*. 2011; Tseng, Albrecht and Gunsalus 1996) and cytochrome *bd*-II is expressed during stationary phase and phosphate stress (Borisov *et al.* 2011; Tseng, Albrecht and Gunsalus 1996).

1.4.3 *E. coli* terminal oxidases

1.4.3.1 Cytochrome bo'

Cytochrome *bo'* is part of a haem-copper terminal oxidase superfamily, it functions as a redox-driven proton pump because it reduces oxygen to water. In addition, to being controlled by global regulators ArcA and Fnr, (Cotter *et al.*1997) and occurs mainly in high oxygen conditions. Cytochrome *bo'* has four subunits that is encoded by the operon *cyoABCEDE*. *CyoE* encodes a haem *o* synthase which is needed for structural purposes (Borisov *et al*. 2011). The main subunit at the core of this complex binds low spin haem *b* encoded by *cyoB* to a haem-copper bi-nuclear centre where a high spin haem *o* and copper are tightly coupled (Borisov *et al.* 2011), which is where oxygen chemistry occurs. *CyoA* encodes a second subunit, which is important for transferring electrons from ubiquinol to haem *b* as well as substrate binding (Borisov *et al*. 2011). The fourth and fifth subunits, encoded by operon *cyoC* and *cyoD* are thought to be needed for correctly folding subunit I (Borisov *et al*. 2011).

1.4.3.2 The bd-type cytochrome oxidases

The *bd*-type cytochromes are quinol oxidases that couple the oxidation of ubiquinol to form a proton gradient and oxygen reduction (VanOrsdel *et al*. 2013). It comprises of a *CydAB* core dimer and two accessory single-transmembrane subunits, *CydX* and *CydH* (Safarian *et al.* 2019). *E.coli* cytochrome *bd*-I and *bd*-II show sequence homology as well as binding to the same cofactors (Borisov *et al*. 2011; Puustinen *et al*. 1991;VanOrsdel *et al.* 2013). Cytochrome *bd*-I is encoded by *cydABX* and *cydH*, whereas *bd*-II is encoded by the *appCBX* operon. Both are unable to pump protons but can generate a PMF by vectorial proton translocation linked to quinol oxidation (VanOrsdel *et al*. 2013; Borisov *et al*. 2011; Puustinen *et al*. 1991). The PMF can then be used for ATP synthesis by ATP synthase. This makes it less electrogenic than cytochrome *bo'* with the ratio of H^+/e^-=1, whereas a ratio of 2 for cytochrome *bo´* (Puustinen *et al*. 1991). However, cytochrome *bd*-I has a higher attraction for oxygen, thus operates at higher efficiency under microaerobic conditions, whereas when carbon and phosphate levels are low *bd*-II is induced (VanOrsdel *et al*. 2013). Additionally, cytochrome *bd*-I is tolerant to nitric oxide (Borisov *et al*. 2011; Mason *et al.* 2009; Shepherd *et al.* 2016), a respiratory inhibitor that is created by the host in response to infections encountered.

The composition of cytochrome *bd*-I found in *E. coli* is similar to of cytochrome *bd-I* in *Geobacillus thermodenitfificans* (Figure 1.7). Both oxidases have two major transmembranes *CydA* (subunit I) and *CydB* (subunit II), also present within the structure is a small transmembrane helix (*CydX* in *bd-I* or *AppX* in *bd-II*) (VanOrsdel *et al*. 2013; Figure 1.6). The helix is shown to be needed for oxidase activity (VanOrsdel *et al.* 2013; Figure 1.7). This is linked to subunit I next to the Q-loop where ubiquinol binds in *CydA* (Safarian *et al.* 2019; Figure 1.7). The Q-loop can vary in length, in *E. coli* a long Q-loop is seen whereas in *G. thermodenitfificans* the Q-loop is shorter (Theβeling *et al.* 2019). A Q-loop is said to be part of quinone binding and oxidation (Theβeling *et al.* 2019). A single small transmembrane, *CydS* is found on *CydA* in *G. thermodenitfificans* and two are seen in *E. coli*, *CydH* and *CydX* (Safarian *et al.* 2019; Theβeling *et al.* 2019; Figure 1.7).

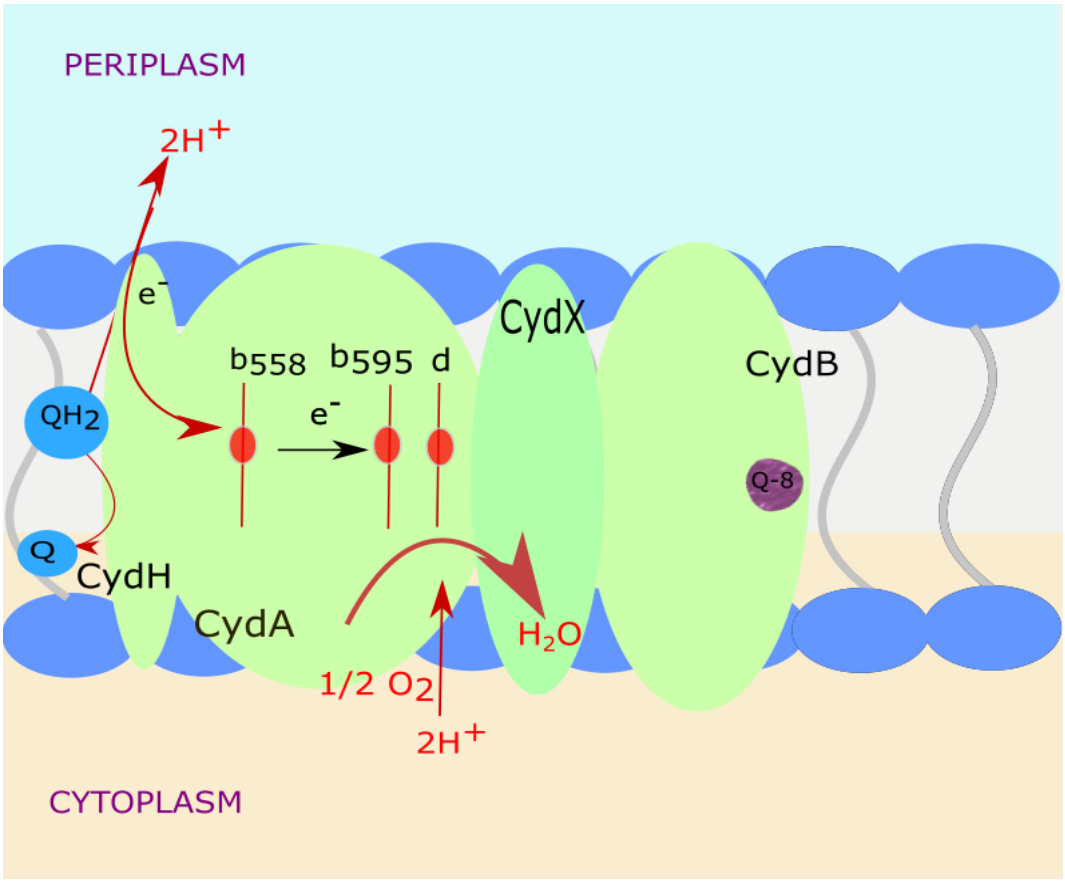

Figure 1.6 Schematic diagram of cytochrome *bd-I* from *E. coli.* Where O_2 is reduced to H_2O using quinol as a reducing substrate. The oxygen reduction is limited to *CydA*, which includes all the three haem cofactors and a periplasmically Q-loop that is exposed. The small proteins *CydX* and *CydH* are additional subunits needed for the enzyme to function. *CydX* is found in front of *CydA*, whereas *CydH* is found behind it. Q-8 represents ubiquinone-8 found in *CydB*.

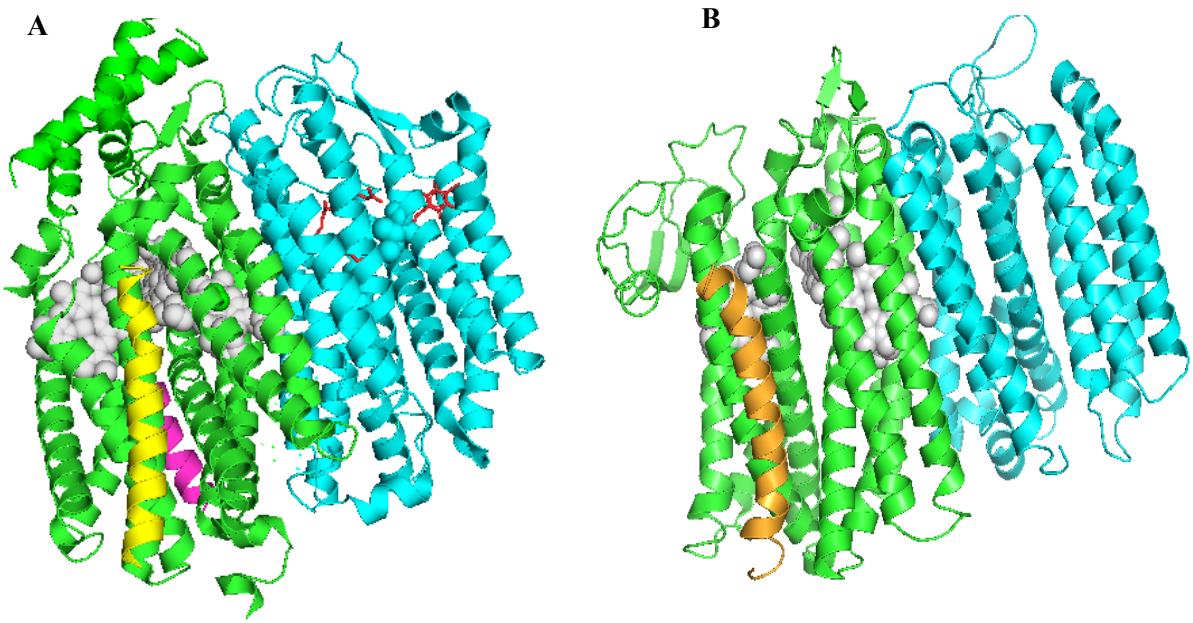

Figure 1.7 Structural model of *bd-I* from *E. coli* (A) and *G. thermodenitfificans* (B). Cytochrome *bd-I* in *E. coli* (6RKO) and *G. thermodenitfificans* (5DOQ) are shown to be nearly identical, however *E. coli* is shown to have another small subunit, *CydX*. Each colour represents a different subunit. Both structures display the haems in subunit I (green).

Cytochrome *bd*-oxidases does not contain copper but three haem cofactors: 2 *b*-type haems (b_{558} and b_{595}) and haem *d* (Giuffrè *et al*. 2014; Figure 1.6). Haem b_{558} is found in subunit I, participating in the oxidation of haem *d* and quinol, where O_2 binds and is reduced to H_2O, other gaseous ligands (CO and NO) bind there also (Giuffrè *et al*. 2014; Figure 1.6). The role of haem b_{595} is uncertain but with haem *d*, a functional binuclear active site is proposed to be formed where reduction of oxygen occurs (Borisov *et al*. 2011; Giuffrè *et al*. 2014). This enzyme is characterised by having high affinity for O_2 so its preferentially expressed in microaerobic conditions (Giuffrè *et al*. 2014). The two auxiliary subunits, *CydX* and *CydH*, are single spanning membrane proteins (Safarian *et al*. 2019). The transmembrane domain (TMD) of *CydX* consists of 37 residues which can be found in a groove formed by TMD 1 and 6 of *CydA* (Safarian *et al*. 2019). *CydH* is a subunit that has been newly identified, with a mass of 3 kDa and is present in a cleft between TMD1 and 9 of *CydA* (Safarian *et al*. 2019). Both *CydX* and *CydH* are non-catalytic but may be vital for the assembly or stability of the oxidase complex (Safarian *et al*. 2019). *CydB* has a structure called ubiquinone-8 in a hydrophobic pocket (Safarian *et al.* 2019; Theβeling *et al.* 2019). Ubiquinone-8 is less likely to be involved in the oxygen reduction or electron transfer, however it may have a structural role in the *CydAB* dimer assembly (Safarian *et al*. 2019; Theβeling *et al.* 2019).

Bd-type oxidases are expressed in various bacterial pathogens including *Salmonella*, *Mycobacteria* and *Streptococcus* (Giuffrè *et al*. 2014). It has been shown to promote virulence and plays a part in the survival and growth of some pathogens it is expressed in (Giuffrè *et al*. 2014). The *bd*-type oxidases play an important role in the protection of bacterial cells against nitrosative and oxidative stress conditions (Giuffrè *et al*. 2014). An example is *Shigella flexneri*, where intracellular survival and virulence was positively correlated to cytochrome *bd*-expression levels (Giuffrè *et al*. 2014). Given that *bd*-type oxidases are only found in prokaryotes, this suggests that these respiratory complexes can be potential drug targets. Most pathogens that can cause severe virulent diseases such as *salmonella* rely on long Q-loop *bd*-oxidases for their survival (Safarian *et al*. 2019).

1.4.4 Nitric oxide, respiratory inhibition, and antimicrobial lethality

1.4.4.1 The role of nitric oxide in the immune system

Nitric oxide (NO) is a free radical gas as well as a vital biomolecule. It has many functions in the human body such as being part of the signal transmission between cells, circulation, cardiovascular system, and immune response (Rőszer 2012). Macrophages produce NO in response to bacterial pathogens (Rőszer 2012). NO can also be synthesised by inducible nitric oxide synthase, which converts L-arginine into NO and citrulline in the presence of oxygen (Alderton, Cooper and Knowles 2001; Rőszer 2012).

Mammalian cells act in response to pathogen invasion by activating proteins that cause a burst of nitrosative and oxidative stress (Baptista, Justino, Melo, Teixeira and Saraiva 2012). In turn, NO can form different reactive nitrogen and oxygen species such as peroxynitrite ($ONOO^-$) from the interaction of ROS superoxide (Baptista *et al.* 2012). This can have a bactericidal or bacteriostatic effect on phagocytosed organisms (Poock, Leach, Moir, Cole and Richardson 2002).

NO has low toxicity to mammalian cells but provides potent bactericidal effects. This can be used as a potential therapeutic to combat bacterial infections. However, many pathogens shield themselves from the effects of NO by initiating a selection of detoxifying enzymes (Baptista *et al.* 2012).

1.4.4.2 Nitric oxide modulates antimicrobial toxicity

Bacteria can be protected from the effects of antibiotics when exposed to NO. It diminishes the toxicity from a variety of mechanisms such as the reduction of oxidative stress, inhibition of respiratory activity and structural changes of the drugs (Gusarov, Shatalin, Starodubtseva and Nudler 2009; Holden *et al*. 2013; McCollister, Hoffman, Husain and Vázquez-Torres 2011). NO from bacterial NOS (bNOS) increases resistance of bacteria to antibiotics which enables them to survive. Acriflavine (ACR) an antimicrobial was shown to have a change in structure by the addition of NO (Gusarov, Shatalin, Starodubtseva and Nudler 2009). The two aromatic amino groups present in its structure allow it to be toxic, the addition of NO led to the formation of gas and a colour change, suggesting a change in structure (Figure 1.8; Gusarov, Shatalin, Starodubtseva and Nudler 2009). This modification of ACR by the exposure to NO led to a decrease in killing of *B. subtilis* and *Staphylococcus aureus* by a less toxic dihydroxyacridine derivative being formed via nitrosylation of the arylamino group (Gusarov, Shatalin, Starodubtseva and Nudler 2009). This effect only reduces the toxicity partially, suggesting that efficient protection against ACR involves additional mechanisms. NO has also effectively diminished the activity of Lactam toxicity against *B. subtilis* indirectly by suppressing oxidative stress via cellular response mechanisms. The reduction of oxidative stress is likely to be linked to the diminished respiratory activity in the presence of NO.

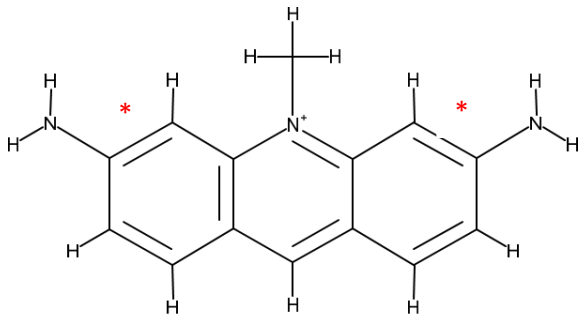

Figure 1.8 Chemical structure of acriflavine. The two asterisks show the two aromatic rings with the amino group, which provides the toxicity.

Given that the loss of the aerobic respiratory chain in *E. coli* results in diminished lethality of a variety of antibiotics (Lobritz *et al*. 2015), it is likely that NO-mediated respiratory inhibition may also have a profound effect upon the efficacy of antibiotics. NO has been

shown to have an inhibitory effect on the ETC, therefore an effect on respiration by the nitroylation of haem *d* activity of terminal quinol cytochrome oxidase due to its high affinity (McCollister, Hoffman, Husain and Vázquez-Torres 2011). This blocks the electron transport and translocation of protons across the membrane needed for the uptake of aminoglycosides, therefore decreasing its efficacy and protection against structurally diversed classes of aminoglycosides (McCollister, Hoffman, Husain and Vázquez-Torres 2011). Thus, allowing bacteria such as *salmonella* to survive. This inhibitory effect of NO was also seen with the addition of gentamicin, which promoted the resistance of *Pseudomonas aeruginosa* and *Staphylococcus aureus* (McCollister, Hoffman, Husain and Vázquez-Torres 2011).

While NO is a potent respiratory inhibitor, *E. coli* possesses cytochrome *bd*-I which allows it to be resistant to NO. This is due to the unusually high *off* rate for NO (Mason *et al.*2009), which promotes survival under conditions of nitrosative stress (Shepherd *et al.* 2016). Given the different sensitivities to NO of the various terminal oxidases of *E. coli*, it would seem likely that each would have a different contribution to antimicrobial toxicity in the presence and absence of NO (which is found during infection). This represents the main hypothesis that is tested in the current work.

1.5 Hypotheses and research techniques

Hypothesis 1 – Cytochromes *bd*-I and *bd*-II of *E. coli* can be measured using difference spectroscopy on a conventional spectrophotometer. To validate a suite of terminal oxidase mutants as a viable tool for this study, expression of *bd*-type oxidases will be detected in membrane preparations using CO difference and reduced *minus* oxidised spectroscopy**.**

Hypothesis 2 –Does NO inhibition of terminal oxidases lead to a disrupted PMF in *E. coli*. With the use of the Wild-type strain, the electrical component of the PMF will be measured using the fluorescent dye $DISC_3(5)$.

Hypothesis 3 - NO will modulate the efficacy of bactericidal drugs. Dose response viability assays will be employed to measure the impact of NO upon bactericidal drugs.

Hypothesis 4 - The terminal oxidases of *E. coli* will affect drug susceptibility in different ways. Dose response viability assays will be used on a suite of terminal oxidase mutants to measure the impact of NO upon bactericidal drugs, and the effect of each terminal oxidase to this lethality.

Chapter 2

Materials and Methods

2.1. Bacteriological Methods

2.1.1 Plasmids and bacterial strains

The plasmids and bacterial strains used during this research are recorded in the tables below. The bacterial strains are all derivatives of *E. coli* clonal group ST131 strain EC958. The plasmid maps are also seen below in Figure 2.1.

Table 2.1 Plasmids used

Plasmid	Description	Antibiotic resistance	Parent strain
pCP20-Gm	10,030 bp; Expresses Flippase; Temperature sensitive (ts) replicon	Ampicillin, Gentamicin	MS107
pKOBEG-Gm	8,264 bp; Expresses λ-red machinery	Tetracycline, Gentamicin	MS11

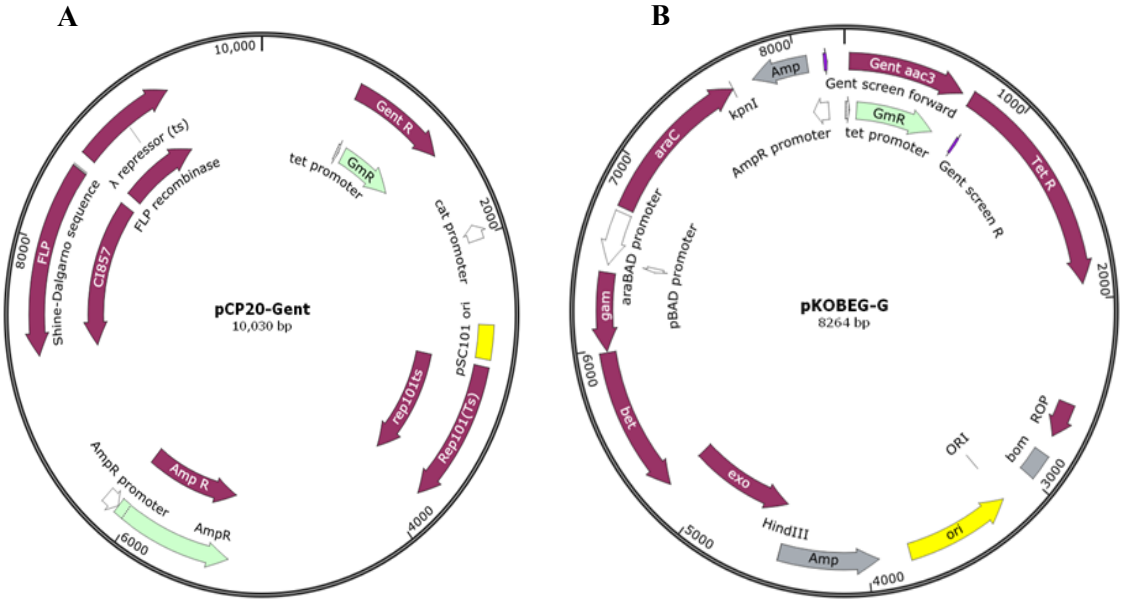

Figure 2.1 Plasmid maps of A) pcCP20-Gm B) pKOBEG-Gm

Table 2.2 Oligonucleotides used during PCR screening

Primer number	Name	Sequence	Use	Direction
299	AmpR_R	GCGATCAAGGCGATTACATGATCCCCCATGTTGTGCAAAAAAGCGGTTA	Screen presence of pCP20_gm plasmid	
389	SpCP20_R	GTAATTGTCCTTTTAACAGCGATCGCGTATTTCGTCTCGCTCAGGCGCAA	Screen presence of pCP20_gm plasmid	
418	pKOBEG_Sc_R	ATCATCGCCATTGCTCCCCAAATAC	Screening primer to detect pKOBEG	Reverse
419	pKOBEG_Sc_F	TGGGCTAGCGAAAAGATGTTTCGT	Screening primer to detect pKOBEG	Forward

Table 2.3 Bacterial strains

Strain	Genotype	Plasmid	Antibiotic resistance	Reference
MS10	WT	-	ESBL	Lau *et al*. 2008
MS11	WT	pKOBEG_Gm	ESBL, Gm, Ap	Shepherd laboratory
MS107	WT	pCP20_Gm	ESBL, Gm, Tet	Shepherd *et al*. 2016
MS628	*cyoA appCB*::Cm^R	-	ESBL, Cm	Ayrianna Woody
MS629	*cydAB appCB*::Cm^R	-	ESBL, Cm	Ayrianna Woody
MS630	*cydAB cyoA*::Cm^R	-	ESBL, Cm	Ayrianna Woody

2.2 Chemicals

Chemicals used during this study were obtained from Sigma unless indicated. Nutrient agar, yeast extract and tryptone were acquired from Oxioid. Milli-Q and deionised water was used during this study. Components used that needed to be sterilised were autoclaved

at 121°C, 15 psi for 15 min. Furthermore, filter sterilisation was also conducted using Millipore filters (0.22 µm pore size).

2.3 Buffer and media solution

2.3.1 Luria- Bertani Medium (LB)

LB medium was made for 1 L, consisted of 10 g of NaCl and tryptone, also 5 g of yeast extract. However, if solid media was needed, then 15 g of nutrient agar was weighed out. For sterilisation the medium was then autoclaved.

2.3.2 M9 Minimal medium

100 mL of M9 medium was made by combining 20 mL 5X M9 salts, 2 mL 20 % (w/v) glucose, 10 µL 1M $CaCl_2$, 200 µL 1M $MgSO_4$, 5 mL 2% (w/v) casein hydrolysate in 72.79 mL of autoclaved deionized water. This was then filter-sterilised and stored at 4°C.

5X M9 salts was composed of 8.02 g sodium phosphate dibasic dihydrate ($Na_2HPO_2.2H_2O$), 1.5 g potassium phosphate monobasic (KH_2PO_4), 0.5 g ammonium chloride (NH_4Cl) and 0.25 g of NaCl was added to 100 mL deionised water. Which was mixed thoroughly, autoclaved for sterilization, and stored at 4°C.

2.3.3 Phosphate- Buffered saline (PBS)

One tablet (oxiod Dulbecco A) was added to 100 mL deionized water to make 1X PBS solution. For sterilisation it was autoclaved after the tablet completely dissolved.

2.3.4 Tris- Acetate- EDTA (TAE) buffer

50X solution of TAE buffer comprised of 242 g Tris base, 57.1 mL acetic acid and 100 mL of 0.5M EDTA to 900 mL deionised water. The solution of 1X TAE buffer was made by the addition of 20 mL of 50X buffer to 980 mL of deionised water.

2.3.5 Sonication buffer

500 mL of sonication buffer was made, which contained 2 mM of magnesium chloride hydrate ($MgCl_2.6H_2O$), 20 mM of TRIS-HCl at pH 7.4 and 1mM EGTA. This was either autoclaved or filter-sterilised and kept at 4°C.

2.3.6 HEPES Buffer

1 L of HEPES buffer was made containing 5 mM glucose and HEPES at pH 7.2. This was autoclaved and stored at 4°C. To make the HEPES buffer mixture, 9352.33 µL of HEPES, 1429 µL of DMSO, 476.2 µL of 3 M KCl and 28.57 µL of 1 mM $DISC_3(5)$ was added to give a final concentration of 5 mM HEPES buffer, pH 7.2, containing 5 mM glucose, 100 mM KCl and 2 µM $DISC_3(5)$.

2.4 Antibiotic stock solutions

The table below shows the antibiotic stocks used during this study. All stocks made were filter sterilised and stored in the freezer before being used. Nitrofurantoin powder was dissolved in DMSO on the day it was needed.

Table 2.4 The different antibiotic stock solutions used during the study.

Antibiotic	Stock solution (mg/mL)	Concentration in media (µg/mL)
Ampicillin (in deionised water)	125	25
Chloramphenicol (in 100% ethanol)	34	25
Gentamicin (in deionised water)	30	30
Nitrofurantoin (in DMSO)	100	-

2.5 Growth conditions of bacteria

From a single colony 10 mL of a starter culture was inoculated in LB broth, which was grown at 37°C and 180 rpm overnight, unless stated otherwise in a Brunswick™ Innova 3100 model water bath.

2.5.1 Measurement of optical density of *E. coli* cultures

The cell density of *E. coli* cultures was measured using a Cary 60 UV-vis spectrophotometer (Agilent Technologies) at 600 nm.

2.6 Viability assay

2.6.1 Preparation of *S*-Nitrosoglutathione

GSNO was utilized as a nitric oxide donor, and was prepared as previously described (Mohr, Stamler and Brüne 1996). 0.69 g of sodium nitrite ($NaNO_2$), 3.08 g of reduced glutathione and 0.83 mL 1.18 M HCl was added to 18 mL of deionised water in a foil-wrapped 50 mL conical flask, which was stirred on ice for 40 min. The solution was stirred for an extra 10 mins when 20 mL of acetone was added. The precipitate formed was stored using vacuum filtration in a fume hood and cleaned with 2 mL cold water (x5), 10 mL acetone (x3) and 10 mL diethyl ether (x3). The product was then placed in a desiccator wrapped in foil attached to a vacuum then left to dry overnight, ensuring the $CaCl_2$ beads were dry and white. The dry pink powder obtained was placed into a falcon tube wrapped in foil and kept at -80 ^{o}C for no more than 1 month.

When GSNO was needed it was dissolved in water. The concentration was determined by performing a 1:20 dilution in a cuvette and measuring the OD_{545}. The equation below was used to determine the concentration:

$(A_{545}/\varepsilon_{545})$ x 20 (to account for the 1:20 dilution) = GSNO (M)

Extinction coefficient (ε_{545}) = 15.9 $M^{-1}cm^{-1}$ at 545 nm (Mohr, Stamler and Brüne 1996)

2.6.2 Nitrofurantoin Viability assay

100 µL of overnight starter culture of a chosen strain was inoculated in 10 mL M9 minimal medium (with 0.1 % casamino acids and glucose). Cultures were grown until the OD_{600} was at least 0.3. This was diluted to an OD of 0.125 in 5 mL M9 medium or M9 medium with 15 mM GSNO. The diluted cultures were statically incubated for 30 mins at 37°C. 180 µL of pre-exposed culture was then added to 20 µL of a chosen antibiotic stock solution varying in concentration in a microplate. This was statically incubated for 90 mins and serial dilutions were done in 1X PBS. 5 µL of each concentration and dilution were spotted in triplicates on LB agar for 2 biological repeats. The plates were then incubated overnight

at 37°C and CFU/mL calculations were made. The concentrations of nitrofurantoin used (μg/mL): 0.1, 5, 50, 100, 250, 500, 1000, 2000, 5000 and 10000.

Also, averages for a '100 % survival' control was determined using two controls without nitrofurantoin. For each technical repeat the percent survival data was plotted versus the concentration of nitrofurantoin. Then, using sigma plot the IC_{50} was calculated from sigmoidal graphs generated using the Hill, 4 parameter equation. The IC_{50} was averaged from two biological and three technical repeats, and error bars were formed from the standard deviation.

2.7 GSNO growth curve in aerobic conditions

50 mL of M9 minimal media (0.1 % casamino acid and glucose) contained 0.5 mL of overnight culture of MS10 (WT). The OD_{600} was monitored until it reached 0.125. Cultures were then exposed to either media only, 15 mM or 30 mM of solid GSNO, which was grown in triplicate. The OD_{600} was followed every hour for at least 6 hours and at 24 hours. The same procedure was conducted for the other two double mutants (MS628 and MS629), however without 30 mM GSNO.

2.8 Isolation of Plasmid DNA

To isolate the plasmid pCP20-gm from its parental strain the QIAprep spin Miniprep Kit (QIAGEN) was used from the instructions provided. To elute the plasmid, sterilised deionised water was used. This was stored at -20 °C until use.

2.9 Colony polymerase chain reaction (PCR)

50 μL of sterile water was used to resuspend the colonies. The PCR reactions consisted of 25 μL Q5® High-Fidelity 2X Master Mix (New England Biolabs), 300 nM of each primer, 21μL sterile MQ water in 0.2 mL PCR tube (50 μL total volume) and 1 μL of resuspended colony. The PCR tube was placed in thermocycler programmed to one cycle at 94°C for 5 min, 30-35 cycles at 94°C for 15 seconds, 50-65°C (dependent on the primers' T_m) for 30 seconds, 72°C for 4-5 min, and put on hold at 10°C until it was taken out.

2.10 DNA Electrophoresis

1% (w/v) agarose gel with 0.5 µg/mL ethidium bromide at 30 mL (Sigma) was made with 1X TAE buffer. Condition was 150 mA, 80V, for 40-60 min depending on the migration rate of the dye front. DNA of 5 µL was combined with 1 µL of 6X loading dye (Promega) and was added to the well. Taq PCR reactions could be loaded directly onto the gel without loading buffer. To the first well 5 µL of 1 kb Hyperladder™ (Bioline) was added. UV box was used to capture the images of the agarose gels.

2.11 Transformation of *E. coli* mutant strains with pCP20

The transformation with pCP20-Gm was done using electroporation. This plasmid comprises of a temperature-sensitive replicon, gentamicin-resistance and a flippase (Flp). Flp is used in flp-FRT recombination to remove the chloramphenicol cassette from the chromosome of the mutant strains. Flp recognises the FRT sites present on each end of the cassette and cleaves out the gene (Guzman *et al.* 1995).

To prepare the electrocompetent cells, 500 µL of each overnight culture was used to inoculate 50 mL LB broth containing 25 µg/mL of chloramphenicol. This was then incubated at 37 °C and 180 rpm until the OD_{600} was between 0.4-0.8 and transferred into falcon tubes on ice. The cells were collected via centrifugation at 3000 *xg*, 4°C for 10 min and pellets were resuspended in 10 mL ice-cold 10 % (v/v) glycerol. Cells were harvested and washed with 10 mL ice-cold 10 % (v/v) glycerol another two times and then cells were resuspended in 100 µL of ice-cold 10 % (v/v) glycerol and used for electroporation. 40 µL of the electrocompetent cells was added to 3 µg plasmid + 6µL sterile MilliQ water in cold electro-cuvette, while 9 µL of sterile MilliQ water was used as a control. This was tapped to mix it, dried and put into a Bio-Rad electroporator at the conditions: 200 Ω resistance, 25 µF capacitance, 2450 V and a half-life between 5-5.3 ms. A sterile microcentrifuge tube was used to transfer the cells with 1 mL of LB. For 1 hour, the cells were left to recover at 28 °C and 180 rpm. After, 100 µL of the cells were plated onto pre-warmed LB-gentamicin plates. The remaining 900 µL was pelleted at 5000 rpm for 5 min and plated. The plates were left to incubate overnight at 28°C. When colonies were seen, they were screened using PCR to check for carriage of pCP20.

2.12 Measurement of the electrical component of the proton motive force in *E. coli*

Stocks of 5 mM $DISC_3(5)$ were made by adding 25 mg of the powder to 9.149 mL of DMSO. This was separated into 0.5 mL aliquots and kept at -20°C.

A standard curve was constructed to find the right excitation and emission wavelength of $DISC_3(5)$ to maximise the signal:noise ratio. The gain was adjusted to 1000. Concentrations between 0-2 μm in steps of 0.2 were made using HEPES buffer as the diluent. 200 μL of each concentration was pipetted in triplicates on a microplate. The fluorescence was measured at 37°C using BMG labtech SPECTROstar omega at different excitation and emission filters.

2.12.1 Membrane depolarisation assay

100 μL of overnight starter culture of each strain was inoculated into 10 mL of M9 minimal media (with 0.1% casamino acid and glucose). Two biological repeats were recorded. The cultures were grown until the OD_{600} was approximately 0.125. Then 15 mM of solid GSNO was added or 1 mM 2,4-DNP. Cultures were incubated at 37°C and 180 rpm in a shaking incubator for 3 hrs and 30 mins. The cells were then harvested by centrifugation at 3000 *xg* for 15 mins. Cultures of GSNO were done last to preserve the NO effect. After, cells were resuspended in 1 mL HEPES buffer consisting of 5 mM glucose at pH 7.2. The OD was measured and diluted to 0.2 in HEPES buffer. 250 μL of each concentrated stock was added to the last six rows of the microplate and left on ice, while the HEPES buffer mixture was made (refer to section 2.3.6). 150 μL of the mixture was added in triplicate for each culture. The fluorescence was monitored immediately for 90 seconds at 30 second intervals at an excitation wavelength of 584 nm and an emission wavelength of 655 nm, with a gain of 1000 using BMG labtech SPECTROstar omega. The microplate was shaken at 500 rpm before each cycle at 37.1 °C. After 90 seconds the protocol was paused and 50 μL from the concentrated pool was added to the HEPES buffer mixture for each culture. The fluorescence was monitored for a total of 40 min.

2.13 Detection of cytochrome bd-spectral signals in *E. coli* membranes using difference spectrophotometry

Two 2 L non-baffled conical flasks with 1 L of LB media was inoculated with 10 mL overnight starter culture and grown overnight at 100 rpm and 37 °C (i.e at low aeration).

The cells were harvested at 4000 rpm and 4°C for 20 min. The pellets that formed were resuspended in 25 mL sonication buffer (the composition of buffer is described in section 2.3.5) and transferred to a 100 mL beaker. Sonication of the solution occurred at 15μ six times for 30 s with 30 s rest in between each sonication. To avoid overheating the sample the beaker was submerged in a 600 mL beaker with ice. The sample was centrifuged at 8000 rpm for 15 min, the supernatant was kept, and pellet discarded. Another centrifuge step was conducted for 1 h at 37,000 rpm and 4°c using an ultracentrifuge. The supernatant was discarded, and the pellets were retained and weighed. Pellets were then resuspended in 900 μL sonication buffer using a glass homogeniser and transferred to Eppendorf tubes before 16 mM of sodium cholate hydrate was added and mixed thoroughly.

A Cary 60 UV-VIS spectrophotometer was used to perform the spectral analysis. The sonication buffer was used as the blank for the range of 700-380 nm. 500 μL of the suspended membrane was added to a quartz cuvette and spectra were recorded to gauge whether membrane suspensions required dilution (aiming for absorbance at 380 nm from 1.0 - 1.5). A little amount of ammonium persulphate was added (to generate an oxidised sample) and another spectrum was recorded. An additional, 500 μL of fresh suspended membrane was added to the cuvette with limited grains of sodium hydrosulphite and the spectrum was logged (i.e., a reduced sample). To obtain a reduced-oxidised difference spectrum the oxidised spectrum was subtracted from the reduced. For the CO-difference spectrum the reduced sample had CO bubbled through the solution for 5 min, a spectrum was recorded, and the reduced spectrum was subtracted from this one.

Chapter 3

Results

3.1 Lambda-Red approaches for mutagenesis of respiratory complex loci in *E. coli* EC958

There is a relationship between aerobic respiration and antibiotic susceptibility. Chromosomal mutagenesis is a powerful tool that can be used to investigate this relationship. Previously in the Shepherd lab, a suite of three double mutant strains was developed (Woody 2019) as tools to investigate the individual contributions of each of the three respiratory oxidase complexes cytochrome *bo'*, cytochrome *bd*-I and *bd*-II (each double mutant strain encodes a single oxidase). However, a triple mutant strain lacking all oxidases would be a useful addition to this work, yet such a strain remained elusive. It has been demonstrated that it is possible to knock out all three respiratory oxidase complexes in non-pathogenic *E. coli* strains (Lobritz *et al.* 2015; Portnoy, Herrgård and Palsson 2008). Hence, Lambda-Red mutagenesis tools were used to generate this triple oxidase mutant during this study.

3.1.1 Development of a PCR screening method for the pCP20-Gm and pKOBEG plasmids

Lambda-Red mutagenesis relies upon the successive introduction and removal of two plasmids, pKOBEG and pCP20 (Datsenko and Wanner 2000; Shepherd *et al.* 2016), for promoting recombination and flipping out resistance genes, respectively. However, with the antibiotic resistant EC958 strain used in this study, we are limited with respect to the choice of antibiotic used, so both plasmids therefore contain a gentamicin resistance cassette. Hence, before performing Lambda-Red mutagenesis to knock out the loci that encode respiratory complexes, it was essential to develop a PCR tool to differentiate between the two plasmids. Firstly, a colony-PCR for pCP20-Gm was developed to verify the mutagenesis had worked. Primers were designed to bind to pCP20-Gm that would generate a PCR product of 3899 bp (Figure 3.1). The strain MS107, a wild-type strain encoding the plasmid was used to conduct the screening and was used as the positive control. PCR products of approximately 3899 bp were observed. A second colony PCR was conducted for pKOBEG-Gm, encoding λ-Red machinery, which would be needed to substitute an oxidase gene with a chloramphenicol cassette. This would be performed to replace the last oxidase present, when constructing the triple mutant. Primers were created

to bind to the plasmid to generate a product of 1915 bp. Both colony PCRs showed the positive controls were successful and could be used to detect the plasmids in transformed colonies chosen.

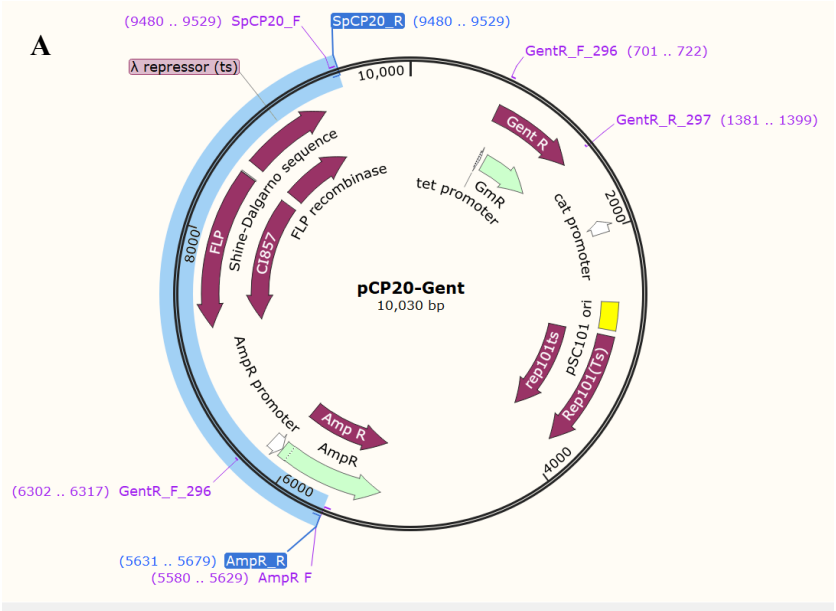

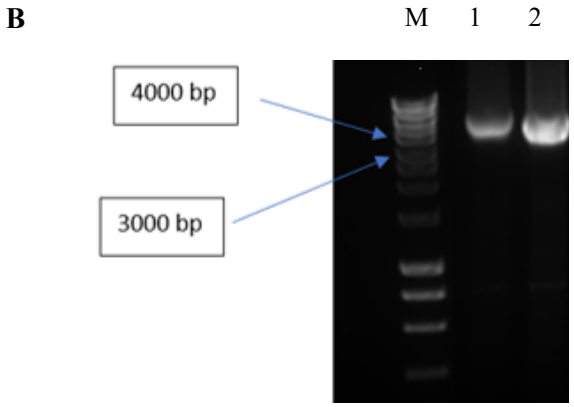

Figure 3.1 Colony PCR development of pCP20-Gm. A) Plasmid map of pCP20-Gm, where forward and reverse primers used are highlighted. B) Screening primers (#299 and #389) was used to confirm the plasmid and would produce a fragment at 3899 bp in 1% agarose gel. Lane M shows Bioline Hyperladder ™ 1kb ladder. Lanes 1-2) Two colonies of MS107.

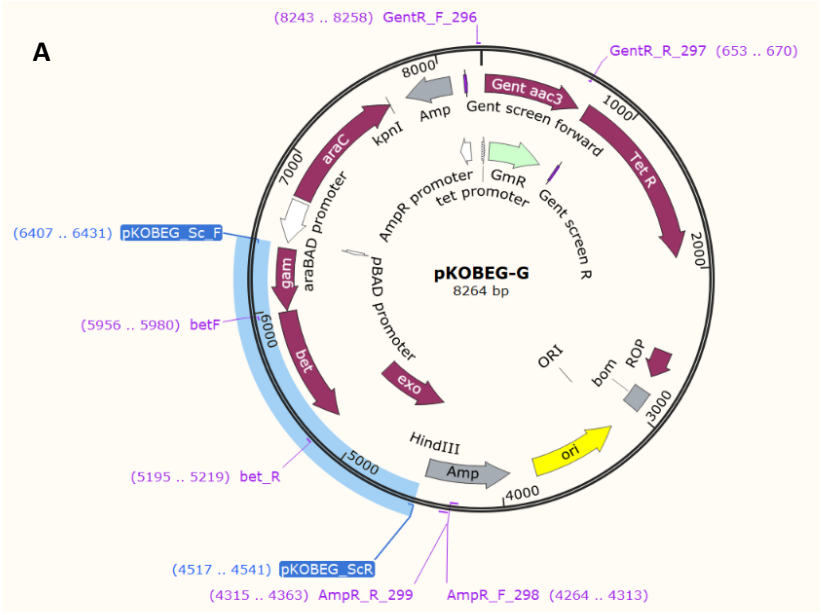

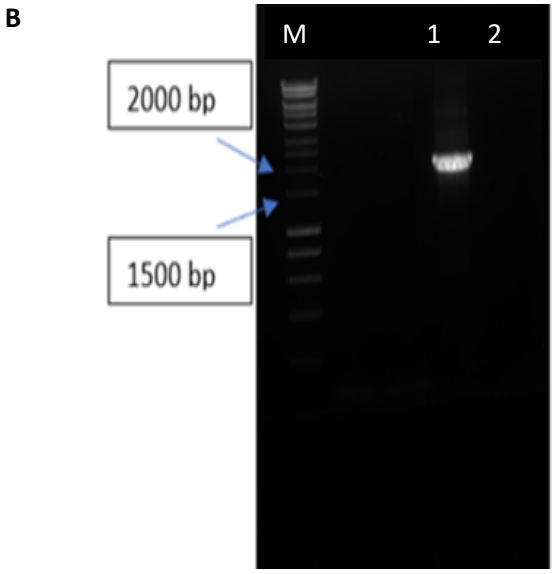

Figure 3.2 Colony PCR development of pKOBEG-Gm. A) Plasmid map of pKOBEG-Gm, where forward and reverse primers are highlighted B) Screening primers (#418 and #419) was used to confirm the plasmid with an expected fragment at 1915 bp in 1% agarose gel. Lane M shows Bioline Hyperladder ™ 1kb ladder. Lanes 1) Colony of MS11 2) Colony of MS628

3.1.2 Attempts to engineer an *E. coli* EC958 triple mutant strain lacking all three respiratory oxidases

The starting point for this work was the three double mutant strains MS628, MS629, and MS630 (Table 2.3) that each encode only one of the three respiratory oxidases. However, these strains each contained a single Cm^R resistance cassette that had to be removed before subsequent mutagenesis could take place (as this relies upon *introduction* of a Cm^R cassette). All three strains were confirmed to be susceptible to Gm and resistant to Cm before this work commenced. The next step was to transform each double mutant using pCP20-Gm to flip out the FRT-flanked chloramphenicol cassette. Following electroporation and plating on LB/Gm, the plates for MS630 appeared to be the most promising with colonies present on the test plate but not on the control plate (Figure 3.3).

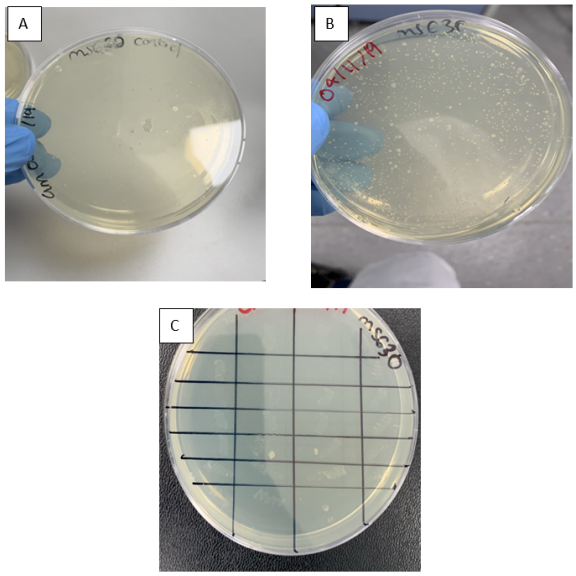

Figure 3.3 MS630 (EC958 cydAB cyoA::CmR) transformation with pCP20. A) Control plate where MS630 was transformed with water and has no growth. B) Test plate where MS630 was transformed with pCP20. C) Single colonies taken from the plate in panel B and patched on a LB-Gm plate.

To confirm that the transformation worked, and the colonies harboured pCP20-Gm, a colony PCR was performed. Two colonies were chosen from the gridded plate seen in Figure 3.3. The MS107 strain encoding pCP20 was utilized as the positive control, and the original MS630 strain was the negative control. However, from Figure 3.4 we see no bands for the potential transformed mutant but only for the positive control. The results suggest that even though the colony PCR worked and was carried out correctly since we see a band for MS107. The lack of bands for the tested colonies suggests that the transformation failed.

This was difficult to explain because the post-electroporation colonies were clearly resistant to gentamicin (Figure 3.3) and the original double mutant strains did not show resistance to gentamicin. At this stage it was hypothesised that the Lambda-Red plasmid, pKOBEG, may have been introduced to the cells. Hence, an additional colony PCR was conducted to determine whether pKOBEG-Gm was present (Section 3.1.1). However, these results showed that pKOBEG was only present in the positive control reaction, suggesting that the gentamycin resistance seen in Figure 3.3 is derived from an unknown source. These experiments were conducted multiple times, and while observation of gentamycin resistance was somewhat reproducible, the presence of pCP20 could not be verified using colony PCR. Dimer primers were also seen, this could be prevented by repeating the PCR with different primers.

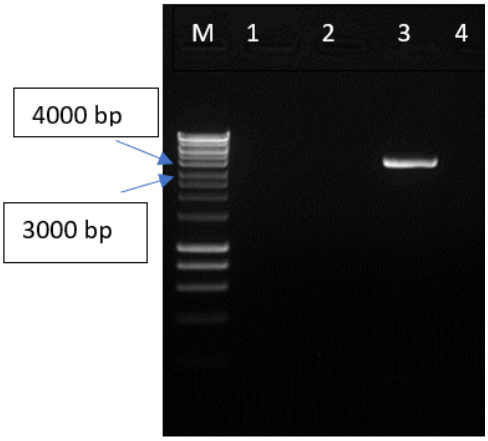

Figure 3.4 PCR screening to detect the presence of pCP20-Gm in transformed *E. coli* MS630. Colony PCR (Section 3.1.1.) with screening primers #299 and #389 was used to screen MS630 (Lanes 1 and 2) and a positive control MS107 (lane 3) for pCP20. Positive control in Lane 3 shows the expected fragment length of 3899 bp, and Lane 4 shoes the negative control with MS630. Lane M shows Bioline Hyperladder ™ 1kb ladder. PCR reactions of 5 µl were loaded onto the 1% agarose gel.

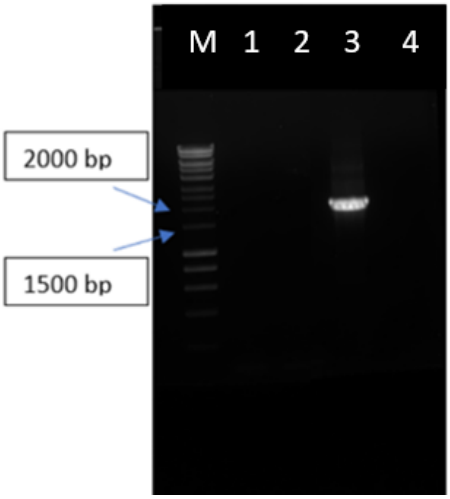

Figure 3.5 PCR screening to detect the presence of pKOBEG in transformed *E. coli* MS630. Colony PCR (Section 3.1.1.) with screening primers #418 and #419 was used to screen MS630 (Lanes 1 and 2) and a positive control MS11 (lane 3) for pKOBEG. Positive control in Lane 3 shows the expected fragment length of 1915 bp, and Lane 4 shoes the negative control with MS630. Lane M shows Bioline Hyperladder ™ 1kb ladder. PCR reactions of 5 µl were loaded onto the 1% agarose gel.

3.2 Detection of *bd*-type oxidase expression/ assembly *E. coli* EC958 respiratory mutants

3.2.1 Development of difference spectra techniques to detect *bd*-type oxidases in isolated membranes using a conventional spectrophotometer

While the creation of the triple mutant failed, we intended to use the single oxidase mutants for further investigation, and it was necessary to check whether *bd*-type oxidases are expressed in these strains. *Bd*-type respiratory oxidase expression is of great importance to the current work, it was of interest to develop a method to measure their abundance in the cell. Spectral signals from haem b_{558}, haem b_{595} and haem *d* from *bd*-type oxidases in *E. coli* have been previously measured in whole cells and isolated membranes using 'reduced *minus* oxidised' and 'CO difference' spectra (Poole *et al*. 1989; Borisov, Gennis, Hemp and Verkhovsky 2011). However, a recent paper reported a method for measuring *bd*-oxidase signals in *E. coli* membranes using a conventional spectrophotometer (Goojani *et al*. 2020), so it was of interest to develop our own protocol for this purpose.

3.2.2 The addition of sodium cholate enhanced the signalling of haem groups present in *E. coli* EC958 in the reduced – oxidised spectrum only

Firstly, membranes from wild type *E. coli* EC958 (MS10) cells were isolated (Section 2.13). Reduced *minus* oxidised and CO-difference spectra were conducted at room temperature using the wild-type strain MS10 to determine if characteristic absorption peaks could be produced. Each cytochrome oxidase has a specific haem group which can be characterised using either 'reduced *minus* oxidised' or 'CO-difference' spectra. Poole et al. (1989) paper was used as a reference to determine each spectral haem peak. Thus, enabling each mutant to be characterised. Haem *d* is only present in *bd*-oxidases, so it's an important feature. Therefore, allowing us to differentiate between each oxidase. Initially, measurements were recorded in the absence of a detergent, which produced spectra of poor quality. Therefore, sodium cholate was added to the isolated membranes to verify if the signal-to-noise ratio could be improved. The reduced *minus* oxidised difference spectra

show three clear peaks with and without the addition of sodium cholate (Figure 3.6). A peak at 633 nm is seen for haem *d* this is caused by the ferrous form of the chlorin haem being reduced (Poole *et al.* 1989; Bloch, Borisov, Mogi and Verkhovsky 2009; Borisov, Gennis, Hemp and Verkhovsky 2011). The peak seen at 558 nm is due to haem b_{558} and contributes to the Soret band seen at 430 nm (Borisov, Gennis, Hemp and Verkhovsky 2011). This peak also leads to overlapping β bands at 527 nm, which is seen slightly (Borisov, Gennis, Hemp and Verkhovsky 2011). The haem peak for b_{595} is a weaker signal but present, nonetheless. The addition of sodium cholate, an important surfactant that acts as a detergent led to increased signal magnitude and clearer peaks.

For the CO-difference spectra, the signal-to-noise ratio was very low, especially in the absence of sodium cholate (Figure 3.7B). The smoothed spectra reveal a peak at 642 nm that is caused by the ferrous haem *d*-CO complex (Figure 3.7B), which is the main feature that is a characteristic of *bd*-type oxidases (Poole *et al.* 1989; Bloch, Borisov, Mogi and Verkhovsky 2009; Borisov, Gennis, Hemp and Verkhovsky 2011). A trough at 622 nm is due to the absorbance bands of high-spin haem *b* and haem *d*. However, the addition of sodium cholate led to these features not being seen (Poole *et al*. 1989; Bloch, Borisov, Mogi and Verkhovsky 2009; Borisov, Gennis, Hemp and Verkhovsky 2011; Figure 3.7C). This could have been caused by CO reacting with sodium cholate which interfered with it binding to specific haem groups present.

3.2.3 Haem absorption spectra for mutant strains expressing single respiratory oxidase complexes

As the procedure used for reduced *minus* oxidised spectra was successful for the wild type strain (***bo´ bd*-I *bd*-II- MS10)**, this approach was repeated for mutant strains expressing only one respiratory oxidase: a cytochrome *bd*-I only strain (*bo´* ***bd*-I** *bd*-II-**MS628**) and a cytochrome *bo´* only strain (***bo´*** *bd*-I *bd*-II-**MS629**). For the *bd*-I only strain we see a peak at 559 nm corresponding to haem b_{558} , and both haems contribute to the Soret band at 427 nm and the β band near 527 nm (Kita, Konishi and Anraku 1984; Figure 3.8). A peak at 560 nm is seen for the '*bo´* only' strain, consistent with previous observations for this oxidase (Kita, Konishi and Anraku 1984). However, the haem *d* peak is less resolved in

bd–I compared to the wild type suggesting a lower level of expression. A minor peak is seen at 595 nm for WT and *bd*–I, which is produced by the high spin b_{595}.

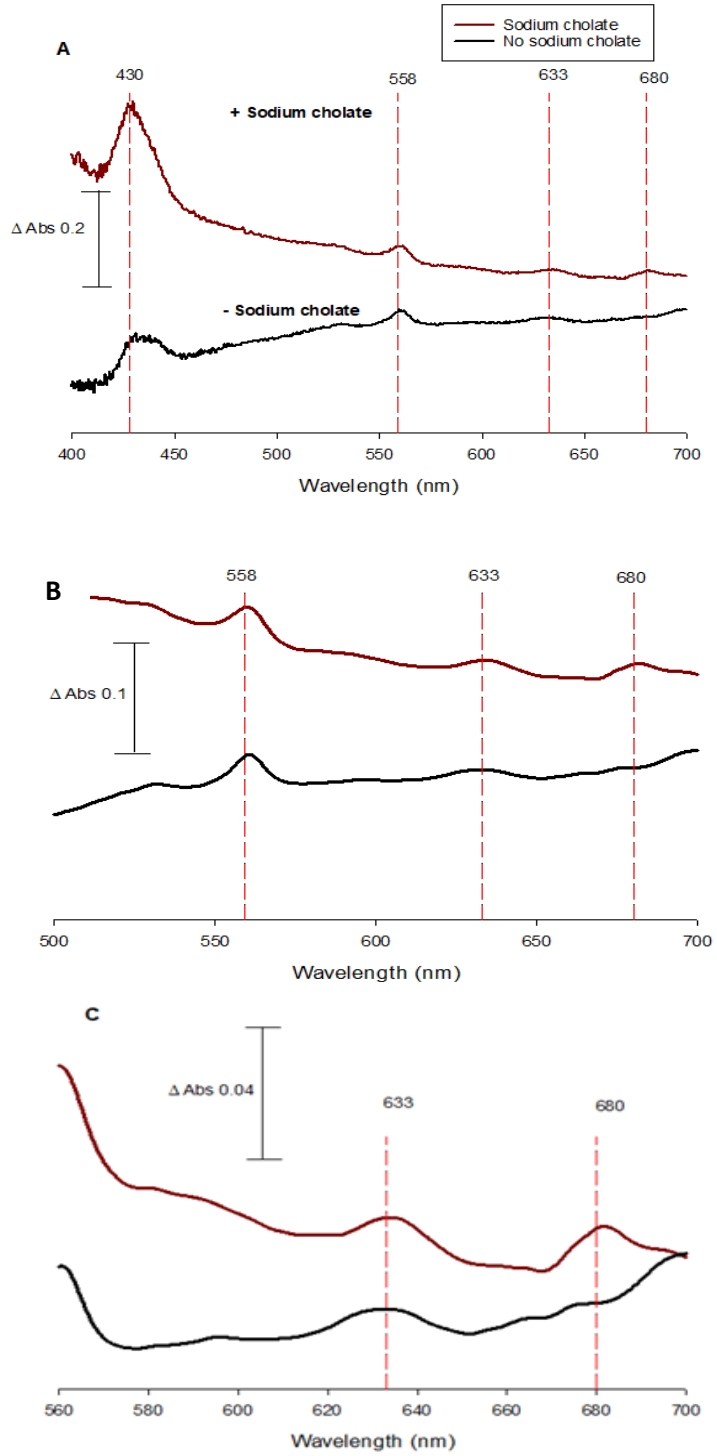

Figure 3.6 Effect of sodium cholate on reduced (dithionite) minus oxidized (persulphate) difference spectra of *E. coli* membranes. A) Raw spectra of MS10 wild-type strain. B) Smoothed spectra from panel A of MS10 (using Sigmaplot). C) Zoomed in view of smoothed spectra from panel B. Concentration of membranes used was 41.92 mg/ml. The scan rate was 300 nmmin^{-1} with data intervals of 0.5 nm (700- 380 nm).

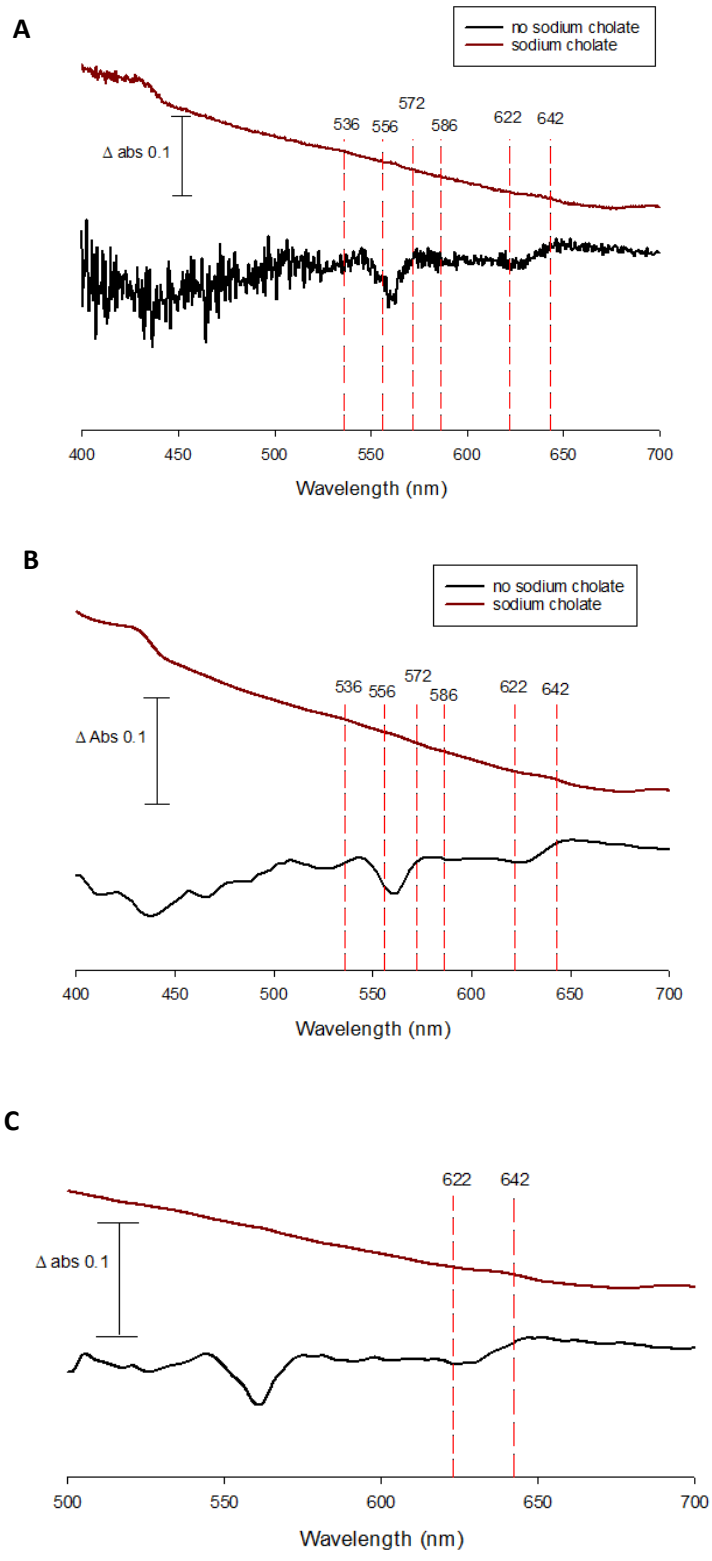

Figure 3.7 Effect of sodium cholate on CO-difference spectra of *E. coli* membranes. A) Raw spectra of MS10 wild-type strain. B) Smoothed spectra (using Sigmaplot) of panel A. C) Zoomed in view of smoothed spectra from panel B. Concentration of membranes used was 41.92 mg/ml. The scan rate was 300 nmmin^{-1} with data intervals of 0.5 nm (700-380 nm).

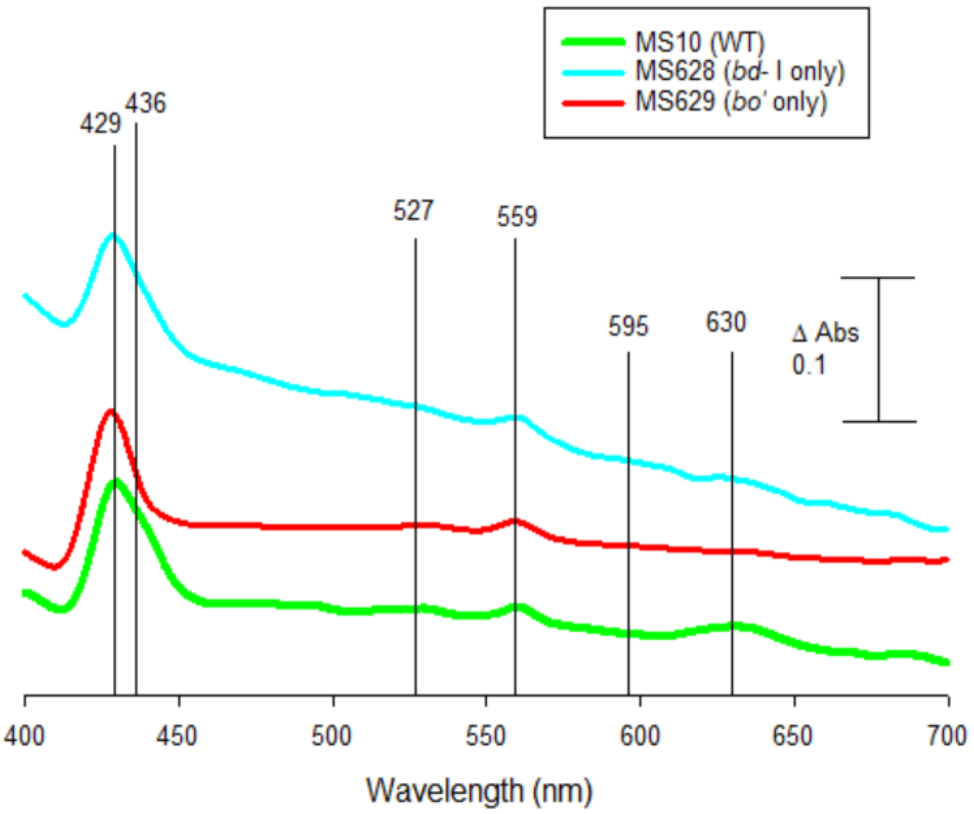

Figure 3.8 - Reduced (dithionite) minus oxidized (ammonium persulphate) difference spectra of *E. coli* mutant membranes. Smoothed spectra (using Sigmaplot) where each line corresponds to an *E. coli* mutant. The concentration of each membranes used was 41.25 mg/ml (WT) 43.80 mg/ml (*bo´* only) and 42.85 (*bd-I* only) The scan rate was 300 nmmin^{-1} with data intervals of 0.5 nm (700- 380 nm).

3.3 Measurement of membrane potential using voltage sensitive dye $DISC_3(5)$

As stated previously, NO is an important biomolecule which is cytotoxic to bacterial cells. It targets terminal oxidases present in the respiratory chain of *E. coli* leading to their inactivation. It was therefore hypothesised that NO would elicit a decrease in proton motive force (PMF). To address hypothesis 2 (Does NO inhibition of terminal oxidases lead to a disrupted PMF in *E. coli*), it was decided that the electrical component of the PMF would be measured using $DISC_3(5)$, a cationic membrane permeable fluorescence dye. The dye accumulates on the membrane of cells with significant PMF and polarised membranes, where the fluorescence is quenched (Te Winkel, Gray, Seistrup, Hamoen, and Strahl 2016; Wu, Maier, Benz and Hancock 1999). Upon dissipation of the PMF and resultant membrane depolarisation, the dye is released into the medium rapidly resulting in alleviation of this fluorescence quenching (Te Winkel, Gray, Seistrup, Hamoen, and Strahl 2016; Wu, Maier, Benz and Hancock 1999). Thus, the disruption to the electrical component of the PMF can be measured by detecting an increase in fluorescence.

Firstly, a standard curve was constructed to determine the optimal excitation and emission wavelengths for $DISC_3(5)$ (Figure B). $DISC_3(5)$ has a maximal excitation wavelength of 622 nm and emission wavelength of 670 nm (Te Winkel, Gray, Seistrup, Hamoen, and Strahl 2016). We used a series of concentrations from 0- 2 μM/mL using HEPES buffer as the diluent. From obtaining the standard curve we found out that an excitation wavelength of 584 nm, an emission wavelength of 655 nm, and a gain setting of 1000 provided us with the best readings. Therefore, these settings were used throughout the PMF experiments.

3.3.1 Optimisation of cell density and dye concentration from PMF measurements

The cell density and the dye concentration are important parameters that influence fluorescence quenching (Te Winkel, Gray, Seistrup, Hamoen, and Strahl 2016). Therefore, a series of cell concentrations were prepared to verify the optimal cell density. From figure 3.9, we see a change in dye fluorescence at all time intervals. The OD values were made by diluting the initial culture to make a series of OD values. The OD_{600} values between 0.01 to 0.075 is where the dye is taken up by the cells due to its negatively charged nature

(quenching) and starts to accumulate within the cells, which explain the decrease in fluorescence readings. At an OD of 0.075, we see an increase in fluorescence suggesting that the additional turbidity may be causing light scattering that may manifest as a higher fluorescence reading. Hence, a concentration of 2 µM $DISC_3(5)$ combined with cells at an OD_{600} of 0.05 was designated optimal for *E. coli*.

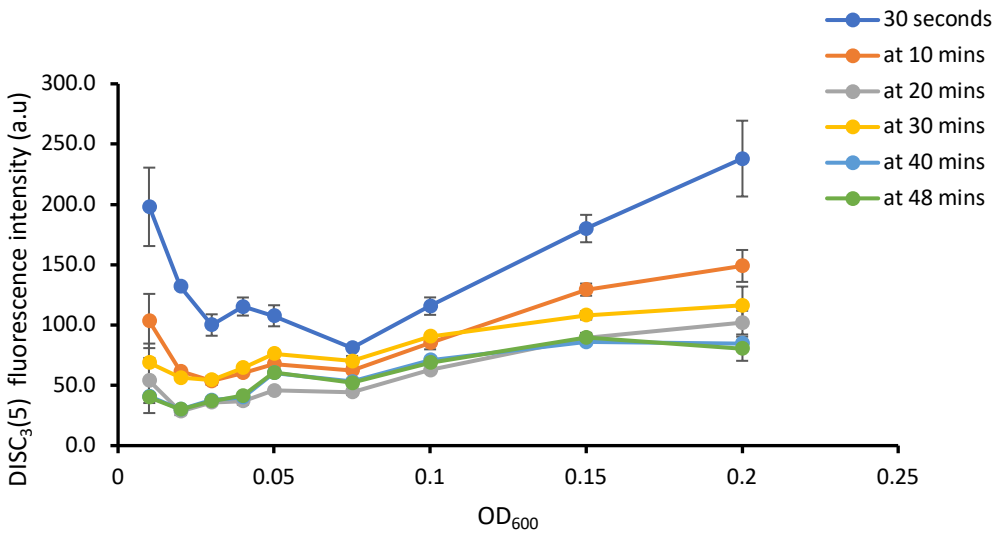

Figure 3.9 Multiple cell concentrations to determine optimal cell density of *E. coli*. A range of concentrations were used to test fluorescence quenching of DISC3(5) over 48 mins using BMG SPECTROstar omega at excitation wavelength of 584 nm and emission 655 nm with a gain of 1000. 3 technical repeats were performed for each concentration. The standard deviation is represented by the error bars.

3.3.2 Investigating interactions between $DISC_3(5)$ and respiratory inhibitors and uncouplers

As the assay focuses on fluorescence quenching, the interaction between the test compounds and dye could potentially influence the measured fluorescence. Therefore, it was important to verify that 2,4-DNP (a membrane uncoupler) and GSNO (a nitric oxide donor) did not drastically change the fluorescence of the dye at the concentrations used. The fluorometric assay was repeated in the absence of cells. 2,4-DNP was shown to be

compatible with $DISC_3(5)$, whereas GSNO led to a dramatic decrease in fluorescence (Figure 3.10A). Hence, the experiment was repeated but GSNO was removed during the wash step (Figure 3.10B), which resolved the issue.

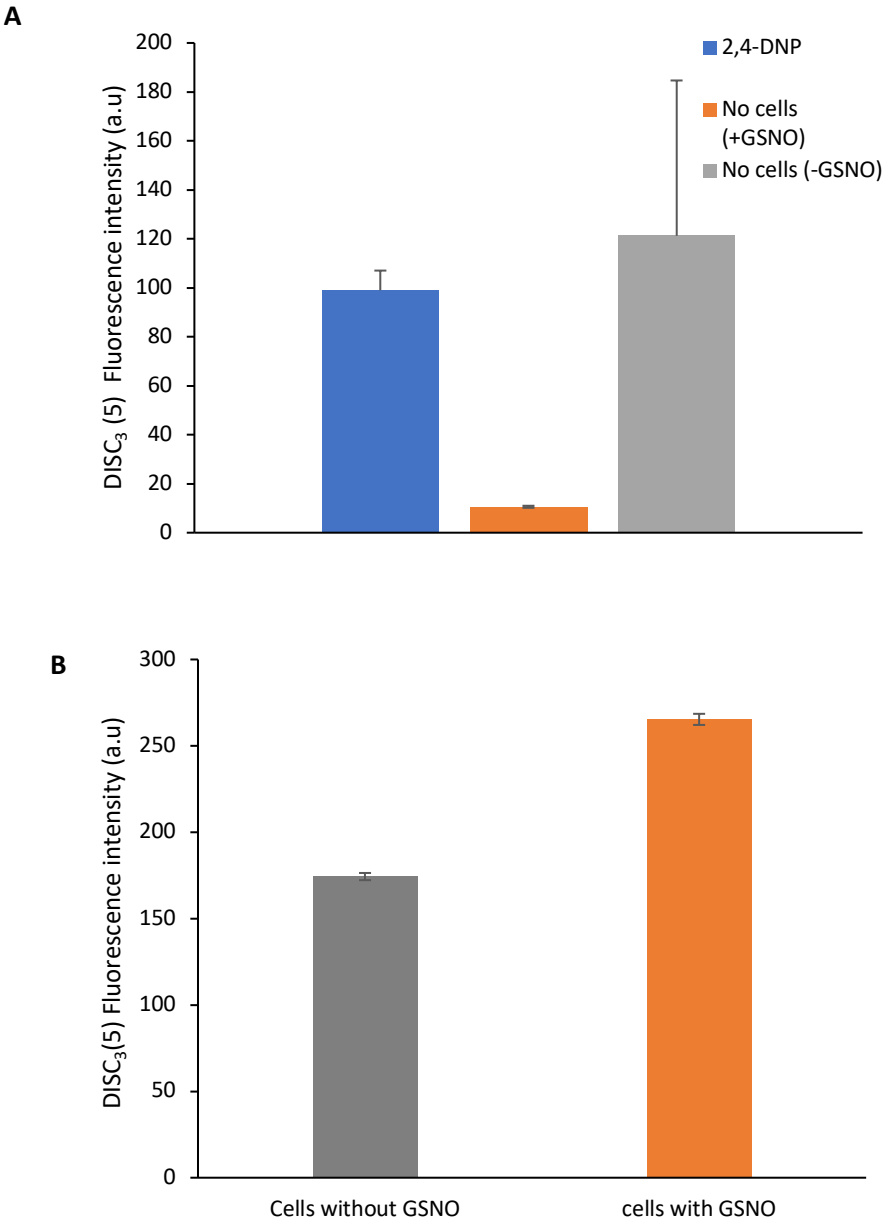

Figure 3.10 GSNO diminished $DISC_3(5)$ fluorescence but can be removed for successful assay of membrane polarisation. A) Fluorescence intensity of 2µM DISC3(5) with the addition of either 1 mM 2,4-DNP (uncoupler) or 15 mM GSNO over 30 mins using BMG SPECTROstar at excitation wavelength of 584 nm and emission 655 nm with a gain of 1000. 3 technical repeats were done for each concentration. B) Conditions of A repeated however with the addition of cells and GSNO removed after the wash step. The standard deviation is represented by the error bars.

3.3.3 Optimisation of GSNO concentrations for *E. coli*

To determine a suitable concentration of the NO-donor GSNO to use in PMF measurements, growth curves were performed. The aim was to find a concentration of GSNO that slowed growth but did not abolish cell division. The addition of 15 mM GSNO, led to a decrease in growth rate (Figure 3.11), but the addition of 30 mM GSNO abolished growth for up to 20 h. Hence, 15 mM of GSNO was used for the PMF measurements and this is consistently used throughout studies conducted in the Shepherd lab. A similar growth curve was performed for the respiratory uncoupler 2,4 – DNP (1 mM), which was shown to be an acceptable concentration as growth rate was diminished but the culture was able to recover in the first 24 h (Figure C).

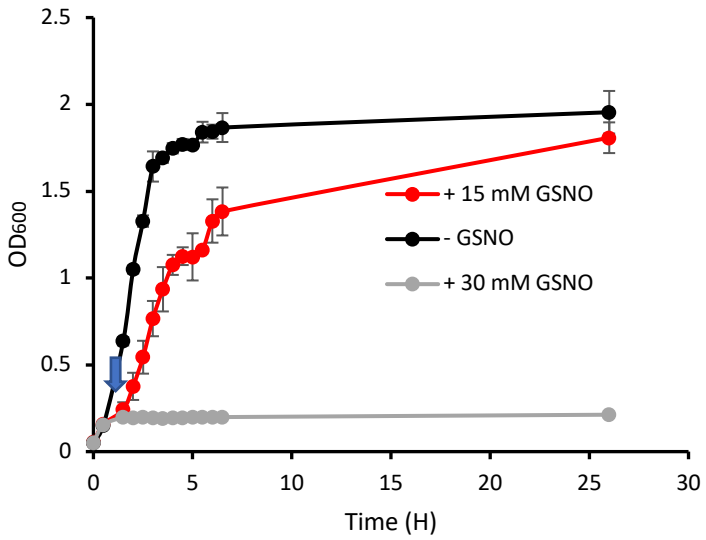

Figure 3.11 Sensitivity of Wild-type *E. coli* strain to GSNO. Cell cultures grown in M9 minimal media (with 0.1% casamino acid and glucose) at 37°C in 250 mL conical flask at 180 rpm for aerobic growth. 15 mM or 30 mM of GSNO was added when the cells reached an OD_{600} of approximately 0.125, this is indicated by the blue arrows. The data point signifies the average of three biological repeats. The standard deviation is represented by the error bars.

3.3.4 GSNO and 2,4- DNP both diminish the membrane potential of *E. coli* leading to an increase in $DISC_3(5)$ fluorescence

2,4-DNP is an uncoupler of oxidative phosphorylation which causes the collapse of the PMF and was therefore used as a positive control (Gage and Neidhardt 1993). The presence of cells (- GSNO and -DNP) led to the dramatic decrease in fluorescence intensity, more than 2-fold (Figure 3.12). This indicates the dye was taken up by *E. coli* cells and the cells have a membrane potential gradient. As shown in figure 3.12, GSNO and 2,4-DNP exhibited similar decreases in membrane potential as shown by the alleviation in fluorescence due to the release of $DISC_3(5)$.

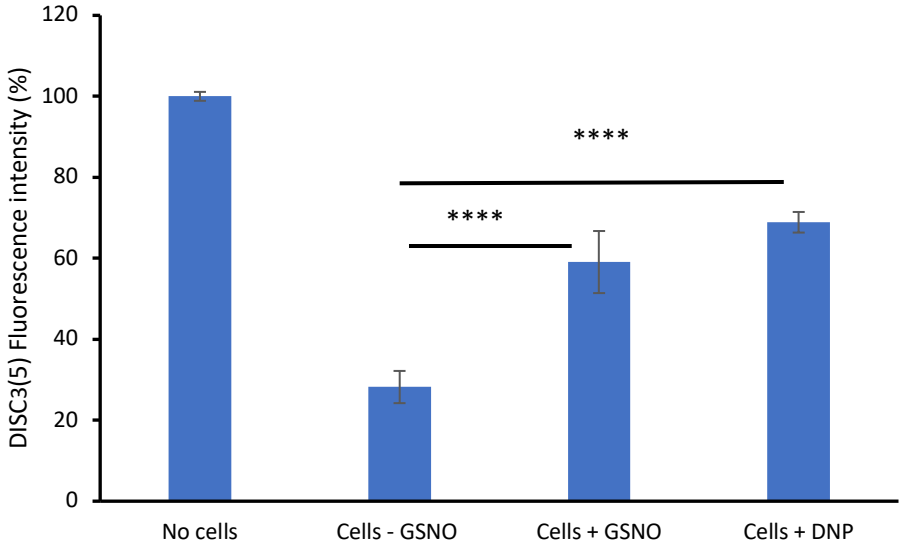

Figure 3.12 Membrane potential of *E. coli* WT in the presence and absence of GSNO and 2,4-DNP using voltage sensitive dye, $DISC_3(5)$. Fluorescence intensity of *E. coli* cells (MS10) were measured using BMG labtech SPECTROstar omega at excitation wavelength of 584 nm and an emission wavelength of 655 nm, with a gain of 1000. Reads were taken for approximately 40 min with cycle times of 30 seconds at 37.1°C in a black microplate. Data represents average from the three repeats from two independent cultures. The error bars seen signifies the standard deviation. (Student's unpaired t-test *$p<0.05$; **** $p<0.0001$).

3.4 Exploring the link between nitrofurantoin susceptibility and NO-mediated respiratory inhibition

It is reported that positively charged aminoglycosides such as gentamicin rely upon the PMF to gain entry to bacterial cells (Bryan and Kwan 1983; Ezraty *et al.* 2013; Woody 2018). Like gentamicin, nitrofurantoin (NF) is also positively charged so it was hypothesised that the PMF may assist its entry into cells. Work conducted previously in the Shepherd lab has shown that the inhibition of bacterial respiration by NO using GSNO lead to a decrease in the efficacy of the aminoglycoside gentamicin (Ribeiro 2018; Woody 2019). Hence, one might expect the respiratory inhibitor NO to have a similar effect upon nitrofurantoin toxicity as has previously been seen for gentamicin. Viability assays were undertaken to investigate this using strains that expressed only one respiratory oxidase: wild type ST131 EC958 (***bo′ bd*-I *bd*-II**), a cytochrome *bd*-I only strain (*bo′* ***bd*-I** *bd*-II), and a cytochrome *bo′* only strain (***bo′*** *bd*-I *bd*-II).

3.2.1 NO increases the efficacy of nitrofurantoin

Previous studies have shown that diminished aerobic respiration reduces the toxicity of antibiotics that are bactericidal (Kohanski *et al*. 2007; Lobritz *et al*. 2015), and it is well known that NO (which is generated by the immune system during infection) is a potent inhibitor of aerobic respiration. Since nitrofurantoin is used to treat UTIs, and it is well-known that NO is present in the bladder during infection, it would be fascinating to investigate the effect of NO upon nitrofurantoin efficacy. To tackle hypothesis 3 (NO will modulate the efficacy of bactericidal drugs), viability assays were conducted to calculate nitrofurantoin killing of *E. coli* EC958 in the absence and presence of NO. A culture grown to early exponential phase (OD_{600} = 0.3) in M9 medium was exposed to 15 mM GSNO for 30 min. Next, the culture was exposed to different concentrations of nitrofurantoin for 90 min. Surprisingly, the results showed a decrease in IC_{50} in the presence of GSNO suggesting an increase in nitrofurantoin lethality. Therefore, a change in the efficacy of nitrofurantoin is seen, hence the acceptance of hypothesis 3.

To test hypothesis 4 (Terminal oxidases of *E. coli* will affect drug susceptibility in different ways), viability assays were also conducted for '*bd*-I only' and '*bo′* only' strains. The data

showed that *bd*-I and *bo′* only strains were more susceptible to combined treatments of NO and nitrofurantoin compared to the WT (Figure 3.13). The *bo´* only strain was the most susceptible to nitrofurantoin as the IC_{50} was quite low compared to *bd*-I and WT, and the addition of GSNO enhanced the effect of nitrofurantoin by decreasing the IC_{50} by more than 2-folds. The highest IC_{50} was seen for the WT strain suggesting that this strain is more resistant to nitrofurantoin, however there is a significant difference in the presence of NO. As the addition of GSNO led to a decrease in the IC_{50} value suggesting it did in fact influence the efficacy of nitrofurantoin.

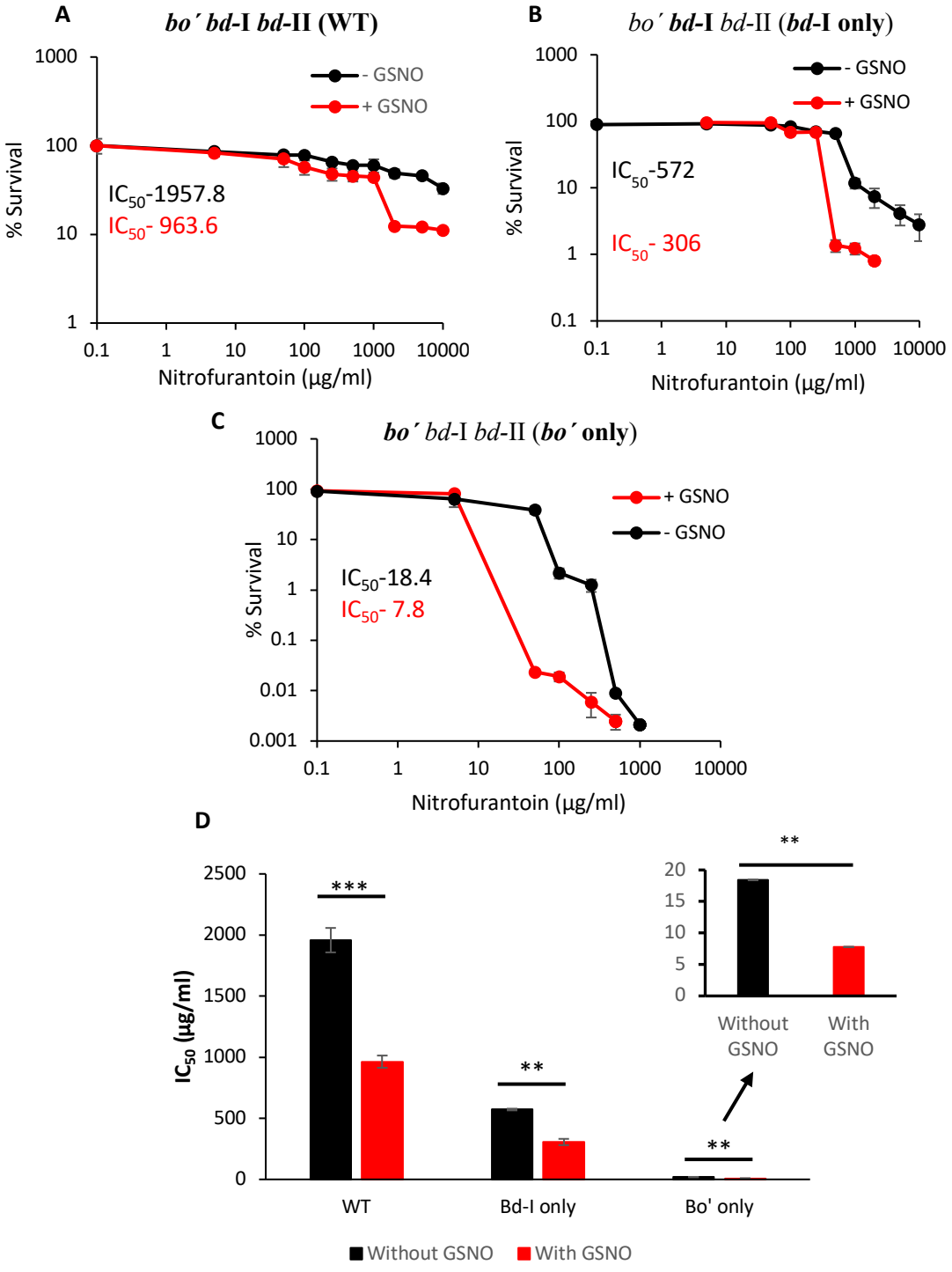

Figure 3.13 Increase in nitrofurantoin lethality in the presence of NO. A-C) Cell survival of WT and mutant strains plotted vs different nitrofurantoin concentration. The mean is shown by the data points and standard deviation of six repeats including two biological repeats. D) IC_{50} of nitrofurantoin +/- GSNO. (Student's unpaired t-test **p<0.005; *** p<0.001).

Chapter 4

Discussion

4.1 Engineering respiratory mutants in *E. coli* EC958

Previous work has demonstrated that it is possible to knock out all three respiratory oxidase complexes in non-pathogenic *E. coli* strains (Lobritz *et al*. 2015; Portnoy, Herrgård and Palsson 2008). Most genetic manipulations of *E. coli* rely on anaerobic growth conditions to be successful (Portnoy, Herrgård and Palsson 2008). However, given that pathogenic strains such as the multidrug-resistant EC958 strain have only 40% of genes in common with K12 strains, it was of interest to engineer respiratory mutants in clinically relevant strain background (Totsika *et al.* 2011).

The first aim of our research was to engineer a triple mutant, which lacks all three terminal oxidases. This would be beneficial in determining whether the removal of the respiratory chain, thus the absence of aerobic respiration would have an impact on antibiotic susceptibility. Studies have shown a *cbd* locus which encodes a putative cytochrome oxidase, however it does not form a functional terminal oxidase (Portnoy, Herrgård and Palsson 2008). Hence, the simple recombineering method adapted from Datsenko and Wanner 2010 was used which involves Lambda Red and flp-FRT recombination to remove the required genes from the chromosome. This technique was successfully done to make the double mutant strains from the Shepherd lab, where colony PCR was performed to ensure the removal of the gene with the addition of chloramphenicol cassettes (Woody 2018).

Double mutant 'single oxidase' strains from the Shepherd lab still retained chloramphenicol cassettes at certain loci, so the first step was to transform the double mutants using pCP20-Gm to express the flippase enzyme to remove the chloramphenicol cassettes (Sarkar *et al*. 2016). Post-electroporation, colonies were present on gentamicin plates. To confirm the presence of the pCP20 plasmid, a PCR screening method was developed with an expected band size of 3899 bp for colonies containing the pCP20. This approach was validated with positive and negative controls using strains known to contain and lack pCP20, respectively (Figure 3.5). However, no PCR product was obtained for the tested colonies, which indicated that the transformation was unsuccessful. This was quite unexpected as the original double mutants were confirmed to be sensitive to gentamicin. One potential explanation for the gentamicin resistance post-pCP20-Gm transformation

would be the integration of the pCP20 gentamicin cassette onto the chromosome, although this would have to include a double recombination event that excludes one or both primer-binding sites. This explanation would seem unlikely given the number of colonies that were obtained. A previous study showed a triple mutant *E. coli* strain was able to grow significantly in M9 minimal medium with a mixture of amino acid but over a long period of time (Portnoy, Herrgård and Palsson 2008). But with the use of LB medium, slow growth was seen (Portnoy, Herrgård and Palsson 2008). Hence, the study may be repeated with different mediums to see which one would lead to significant growth. Due to time constraints, work on the triple mutant was halted and experiments were performed using the single oxidase double mutant strains.

4.2 Detection of *bd*-type oxidase expression in *E. coli* EC958 mutants using a conventional spectrophotometer

E. coli strains with respiratory chain genes deleted have been constructed to study the terminal oxidases (Lobritz *et al.* 2015; Portnoy, Herrgård and Palsson 2008). Here, we showed that the single oxidase mutant strains of *E. coli* EC958 can be exploited for the measurement of *bd*-type oxidase expression using a conventional spectrophotometer. To check whether these strains will be useful for future work on isolated terminal oxidases, it was of importance to check whether the single mutants expressed *bd*-type oxidases as well as the WT. In the past, 'reduced *minus* oxidised' and 'CO difference' spectra have been recorded to quantify terminal oxidase levels in *E. coli* membranes using a dual wavelength spectrophotometer designed for turbid samples (Poole, Williams, Downie and Gibson 1989). The haem groups present on membranes can be differentiated due to their spectroscopic properties. 'Reduced *minus* oxidised' and 'CO difference' spectrums show the difference in absorption between ferrous and ferric forms of a haem-protein (Gennis 1987). The coordination environment of the haem iron including the type of axial ligand, the coordination sphere and coordination number is unique to each haem (Wang, Lu, Yao, Xie, and Huang 2003). Haem *d*, a chlorin which is specific to cytochrome *bd*-oxidase can be used to differentiate between other oxidases present in *E. coli*. Hence, the current work aimed to repeat this work by optimising membrane concentrations and using detergents.

Initial measurements were recorded using a variety of membrane concentrations and above 40 mg/mL (wet membranes) the signal:noise of haem *d* and haem b_{558} peaks diminished in quality, so this was the approximate optimum concentration used thereafter. To aid membrane solubility and further improve signal:noise, sodium cholate was added at a final concentration of 16 mM as previously reported (Goojani *et al*. 2020). From figure 3.6B, we see three clear peaks each corresponding to a haem group. A peak at 633 nm is seen for haem *d* which is caused by the ferrous form of the chlorin haem being reduced. The peak at 558 nm is due to haem b_{558}, which also absorbs at 430 nm (Figure 3.6B). However, a species is seen at 680 nm in the presence of sodium cholate only. Poole and Williams (1988) found a formation of a peak at 680 nm was caused by either hydrogen peroxide being added to persulphate oxidised sample or sample oxidised with ferricyanide and hydrogen peroxide. Hence, the 680 nm species is likely to be due to a peroxy form of haem *d*, the formation of which is potentiated by sodium cholate via an unknown mechanism (Poole and Williams 1988).

The CO difference membrane spectra obtained had a low signal:noise ratio, and the addition of sodium cholate further diminished this. A peak at 642 nm was observed resulting from absorption of the ferrous haem *d*-CO complex, which is the main spectral feature for *bd*- type oxidases (Figure 3.7B). Also, troughs at 622 nm were observed, which result from absorbance of reduced high–spin haem b_{595} and haem *d*. However, with the addition of sodium cholate these features are absent (Figure 3.7B), and further work will be necessary to optimise the 'CO difference' approach.

Analysis of 'reduced *minus* oxidised' spectra for the strains producing single terminal oxidases revealed similar peaks for the '*bd*-I only' strain and the WT (Figure 3.9). The peak seen at 560 nm for '*bo´* only' strain corresponds to an α absorption peak of b_{562}, which is the only cytochrome *b* haem peak present in the strain (Kita, Konishi and Anraku 1984).

Weak signal:noise was a problem seen with all the difference spectra that were recorded, which may be overcome in future by optimisation of the membrane isolation process, or purification of isolated oxidases as previously reported. (Kita, Konishi and Anraku 1984). Other methods such as western blotting or SDS-page can be used to verify the presence of haem groups.

4.3 NO-mediated inhibition of terminal oxidases in *E. coli* EC958 leads to a disrupted PMF

The inhibition of terminal oxidases in *E. coli* occurs due to NO binding (Borisov *et al.* 2004). Since terminal oxidases contribute to the PMF, it is reasonable to assume that NO-mediated respiratory inhibition would lead to disruption of the PMF. The PMF consists of an electrical potential gradient (ΔΨ internal negative) and a pH gradient (internal alkaline) (Wu, Maier, Benz and Hancock 1999). We adopted an assay including the membrane potential sensitive fluorescent dye, $DISC_3(5)$ to assess the disruption of the electrical component of the PMF of *E. coli* EC958 in the absence and presence of nitric oxide donor GSNO. A positive control was also performed using the uncoupler 2,4-DNP.

The optimal cell density was found to be an OD_{600} of 0.05, and this was used with 2 μM $DISC_3(5)$. 1% DMSO was also included as this was vital for ensuring good solubility and fluorescence of the dye. 100 mM of KCl was added to ensure the movement of K^+ ions would not affect the fluorescence, which may resist the dissipation of electrical potential gradient.

Another factor that could impact upon fluorescence quenching is the interaction between the compound of interest and the dye. Hence, it was of importance to ensure 2,4-DNP and GSNO did not directly change the dye fluorescence at the concentration used. We found that 2,4-DNP was compatible with $DISC_3(5)$, although GSNO caused a decrease in fluorescence (Figure 3.10A). This may have been caused by GSNO interacting with the dye as this experiment was performed in the absence of cells. Therefore, after the cells were exposed to GSNO for a certain period, cells were washed to remove the GSNO prior to addition of $DISC_3(5)$.

The exposure of *E. coli* EC958 wild type cells to GSNO led to a significant increase in fluorescence intensity, as was seen with the positive control, 2,4-DNP. A 2-fold increase in fluorescence is seen in the presence of GSNO which is consistent with dissipation of the membrane potential (Figure 3.12). These findings confirm that NO inhibition of terminal oxidases does in fact lead to a disrupted PMF. Although, this may vary between the two single oxidase mutants and wild – type strains, as NO binds to these respiratory oxidases with different affinities (Mason *et al*. 2009). As cytochrome *bd*-I is NO-tolerant, it is still likely to respire in the presence of nitric oxide, therefore the PMF is less likely to be

disrupted (Mason *et al*. 2009). Whereas cytochrome *bo´* is more susceptible to NO-mediated inhibition, so it was anticipated that the PMF of the '*bo´*-only' strain would be dissipated to a great degree. Time constraints precluded the investigation of these additional hypotheses, but it would be of significance to perform these experiments in the future.

4.4 Nitric oxide influences the efficacy of bactericidal drugs

Previously, bactericidal antibiotics have been shown to accelerate the aerobic respiratory chain resulting in the elevation of oxygen consumption and depletion of NADH (Lobritz *et al*. 2015) (Kohanski *et al*. 2007; Lobritz *et al*. 2015). While antibiotics have a range of primary targets, it is thought that this elevated respiratory rate is directly related to cell death. Hence, it is logical that inhibition of the respiratory chain may hinder the efficacy of bactericidal antibiotics. Furthermore, some positively charged antibiotics utilise the PMF for entry into the cell, which is directly generated by aerobic respiration, this adds another explanation why respiratory activity promotes antibiotic-mediated cell death (Allison, Brynildsen and Collins 2011; Baek, Li and Sasseti 2011). As stated previously NO is produced by an immune response in response to bacterial infection and targets the terminal oxidases in *E. coli* resulting in the inhibition of the aerobic respiratory chain. Therefore, leading to a decrease in antibiotic susceptibility in bacteria (Gusarov, Shatalin, Starodubtseva and Nudler 2009).

The presence of NO led to a decrease in gentamicin (a positively charged, bactericidal drug) - mediated killing from conducting a viability assay (Woody 2018). Due to the positive charge on gentamicin, it was speculated that the proton gradient formed via aerobic respiration may be required for entry into the cell which may promote the bactericidal activity of gentamicin (Bryan and Kwan 1983; Ezraty *et al.* 2013). As nitrofurantoin is also a positively charged bactericidal antibiotic it was hypothesised that aerobic respiration would increase antibiotic-mediated bacterial killing, as it the case for gentamicin. Hence, viability assays were conducted in the absence and presence of the respiratory inhibitor NO to investigate the impact upon nitrofurantoin toxicity.

For initial experiments, cells were exposed to 0.1- 1000 μg/ml nitrofurantoin (NF) for 90 min, but no killing was observed. This was conducted several times, with a new batch of

nitrofurantoin but the same observations were made. However, the MIC of nitrofurantoin from zones of inhibition is 64 quite high at μg/mL (BSAC 2013), and NF may only become bactericidal at much higher concentrations. Hence, it was agreed to increase the concentration range to 0.1- 10,000 μg/ml. From figure 3.13A obtained for the WT strain, the exposure to NO decreases the IC_{50} value. This result supports hypothesis 3 as it shows NO modulates the efficacy of bactericidal antibiotics. However, the decrease in IC_{50} suggests NO is not diminishing NF toxicity but is enhancing it. This surprising result is the opposite to what has been observed for gentamicin. For the treatment of UTIs, NF is usually administered at 100 mg twice a day, (Gardiner, Stewardson, Abbott and Peleg 2019), but can accumulate to high concentrations in the bladder (>200 μg/mL), which explains why an antibiotic with a high MIC can be an effective for these particular infections. We can conclude that respiratory inhibition by NO does impact the efficacy of NF so PMF may not be needed for mode of action like gentamicin. This is very interesting as host-derived NO is likely to be promoting NF-mediated killing during the treatment of bladder infections. Previous work has examined the effects of NO and NF in isolation with the hypothesis that NF might release NO during infection (Vumma, Bang, Kruse, Johansson and Persson 2016). This work reported that NO could not be detected during nitrofurantoin treatment of *E. coli* bladder infection, and that NF is much more effective in controlling *E. coli* colonisation that NO alone. However, this study stopped short of performing combinatorial experiments with NO and NF together: the current work has therefore revealed a novel synergistic relationship between NO and NF.

Further investigation of 'single oxidase' mutants showed similar results to the WT. The *bo´* only strain which should be more sensitive to NO-mediated inhibition was killed more readily by the combined treatment of NO and NF compared to WT or the *bd*-I only strain (NO-tolerant) (Figure 3.13; Mason *et al*. 2009). This would suggest that NO-mediated respiratory inhibition might promote NF-mediated killing of *E. coli.* While the molecular mechanism of NF-mediated killing remains somewhat unclear, intracellular nitroreductases are known to reduce nitro groups on NF leading to formation of the active form of the drug (Gardiner, Stewardson, Abbott and Peleg 2019). The current results might suggest that accumulation of electrons in the quinol pool (elicited by NO-mediated inhibition of terminal oxidases) could perhaps promote this reduction process leading to greater bactericidal activity, although further work is required to investigate this hypothesis.

References

1. Alderton, W. K., Cooper, C. E. and Knowles, R. G. (2001). Nitric oxide synthases: Structure, function and inhibition. *Biochemical Journal*, 357(3),593–615.

2. Allison, K.R. et al. (2011). Metabolite-enabled eradication of bacterial persisters by aminoglycosides. *Nature*, 473(7346),216-221.

3. Aminov, R.I. (2009). The role of antibiotics and antibiotic resistance in nature. *Environ Microbiol*, 11(12),2970–2988.

4. Aslam, B. et al. (2018). Antibiotic resistance: a rundown of a global crisis. *Infection and drug resistance*, 2018(11),1645-1658.

5. Baek, S.H., Li, A.H. and Sassetti, C.M. (2011). Metabolic Regulation of Mycobacterial Growth and Antibiotic Sensitivity. *PLOS Biology*, 9(5),2-7.

6. Balasiny, B., Rolfe, M.D., Vine, C., Bradley, C., Green, J. and Cole, J. (2018). Release of nitric oxide by the *Escherichia coli* YtfE (RIC) protein and its reduction by the hybrid cluster protein in an integrated pathway to minimize cytoplasmic nitrosative stress. *Microbiology society*, 164(4),563-575.

7. Bamberg, W.M. et al. (2015). Burden of clostridium difficle infection in the united states. *N Eng J med*, (371), 825-834.

8. Baptista, J.M., Justino, M.C., Melo, A.M.P., Teixeira, M. and Saraiva, L.M. (2012). Oxidative Stress Modulates the Nitric Oxide Defense Promoted by *Escherichia coli* Flavorubredoxin. *Journal of Bacteriology*, 194(14), 3611-3617.

9. Belenky, P. et al. (2015). Bacterial antibiotics induce toxic metabolic perturbations that lead to cellular damage. *Cell Reports,* 13(5),968-980.

10. Blanco, J. et al. (2008). Intercontinental emergence of *Escherichia coli* clone O25:H4- ST131 producing CTX-M-15. *J antimicrob chemother*, 2008(61),273-281.

11. Blass, B.E. (2015). Case studies in drug discovery. *Basic principles of drug discovery and development*. Academic press.

12. Bloch, D.A., Borisov, V.B., Mogi, T. and Verkhovsky, M.I. (2009). Heme/ heme redox interaction and resolution of individual optical absorption spectra of the hemes in cytochrome bd from *Escherichia coli*. *Biochimica et Biophysica acta*, 1787(10), 1246-1253.

13. Bonamore, A., Gentili, P., Ilari, A., Schinima, M.E. and Boffi, A. (2003). Escherichia coli Flavohemoglobin Is an Efficient Alkylhydroperoxide Reductase. *The journal of biological chemistry*, 278(25), 22272-22277.

14. Borisov, V.B ., Gennis, R.B., Hemp, J. and Verkhovsky. (2011). The cytochrome *bd* respiratory oxygen reductases. *BBA- Bioenergetics*, 1807(11), 1398-1413.

15. Bryan, L.E. and Kwan, S. (1983). Roles of ribosomal binding, membrane potential, and electron transport in bacterial uptake of streptomycin and gentamicin. *Antimicrobial agents and chemotherapy*, 23(6), 835-845.

16. Brunning, A. (2014). *An overview of antibiotics*. Longitude prize. Available from: https://longitudeprize.org/blog-post/overview-antibiotics [Accessed 7 October 2019].

17. BSAC. (2013). BSAC methods for antimicrobial susceptibility testing version 12. *British society for antimicrobial chemotherapy*. https://bsac.org.uk/wp-content/uploads/2012/02/Table-6.pdf [Accessed 5 July 2020].

18. Chen, F. et al. (2010) Multiple genetic switches spontaneously modulating bacterial mutability. *BMC Evolutionary Biology*, 277(10),1-11.

19. Choudhuri, S. (2014). *Bioinformatics for beginners: genes, genomes, molecular evolution, databases and analytical tools*. (1st ed.). New York: Academic press.

20. Datsenko, K.A. and Wanner, B.L. (2000). One- step inactivation of chromosomal genes in *Escherichia coli* K-12 using PCR products. *Proceedings of the National Academy of Sciences*, 97(12),6640-6645.

21. Dwyer, D.J. et al. (2014). Antibiotics induce redox-related physiological alterations as part of their lethality. *Proc Natl Acad Sci USA,*111(20),E2100-E2109.

22. Ezraty, B. et al. (2013). Fe-s cluster biosynthesis controls uptake of aminoglycosides in a ros-less death pathway. *Science*, 340(6140),1583-1587.

23. Flatley, J., Barrett, J., Pullan, S.T., Hughes, M.N., Green, J. and Poole, R,K. (2005). Transcriptional Responses of *Escherichia coli* to S-Nitrosoglutathione under Defined Chemostat Conditions Reveal Major Changes in Methionine Biosynthesis. *The journal of biological chemistry*, 280(11), 10065-10072.

24. Forde, B.M. et al. (2014). The complete Genome sequence of *Escherichia coli* EC958: A high quality reference sequence for the globally disseminated multidrug resistant E. coli O25b:H4 ST131 clone. *PLOS one*, 9(8), e104400.

25. Forsberg, K.J. et al. (2014). Bacterial phylogeny structures soil resistomes across habitats. *Nature,*509(7502),612-616.

26. Fourmy, D., Recht, M. I., Blanchard, S. C. and Puglisi, J. D. (1996). Structure of the A site of *Escherichia coli* 16S ribosomal RNA complexed with an aminoglycoside antibiotic. *Science*, 274(5291), 1367–1371.

27. Gage, D.J. and Neidhardt, F.C. (1993). Adaptation of *Escherichia coli* to the Uncoupler of Oxidative Phosphorylation 2,4-Dinitrophenol. *Journal of Bacteriology*, 175(21), 7105-7108.

28. Gardner, A.M., Helmick, R.A. and Gardner, P.R. (2002). Flavorubredoxin, an Inducible Catalyst for Nitric Oxide Reduction and Detoxification in *Escherichia coli*. *The journal of biological chemistry*, 277(10), 8172-8177.

29. Gardiner, B.J., Stewardson, A.J., Abbott, I.J. and Peleg, A.Y. (2019). Nitrofurantoin and Fosfomycin for resistant urinary tract infections: old drugs for emerging problems. *Aust Prescr*, 429(1), 14-19.

30. Gennis, R. B. (1987). The cytochromes of *Escherichia coli*. *FEMS Microbiology reviews*, 3(4), 387-399.

31. Goojani, H.G. et al. (2020). The carboxy-terminal insert in the Q-loop is needed for functionality of *Escherichia coli* cytochrome bd-I. *Biochimica et Biophysica Acta (BBA) – Bioenergetics*, 1861(5-6), 1-30.

32. Guidos, R.J. (2011). Combating antimicrobial resistance: policy recommendations to save lives. *Clin infect Dis,52*(5), 5397-5428.

33. Gusarov, I., Shatalin, K., Starodubtseva, M. and Nudler, E. (2009). Endogenous nitric oxide protects bacteria against a wide spectrum of antibiotics. *Science*, 325(5946), 1380–1384.

34. Hirota, S.A. and Sun, X. (2015). The roles of host and pathogen factors and the innate immune response in the pathogenesis of clostridium difficle infection. *Mol Immunol*, 63(2), 193-202.

35. Holden, J. K., Li, H., Jing, Q., Kang, S., Richo, J., Silverman, R. B. and Poulos, T. L. (2013). Structural and biological studies on bacterial nitric oxide synthase inhibitors. *Proceedings of the National Academy of Sciences of the United States of America*, 110(45),18127–18131.

36. Holmes, A.H. et al. (2016). Understanding the mechanisms and drivers of antimicrobial resistance. *Lancet,* 387(10014),176–187.

37. Imlay, J.A. (2003). Pathways of oxidative damages. Annual review of *Microbiology*, 2003(57),395-418.

38. Karlinsey, J.E. et al. (2012). The NsrR regulon in nitrosative stress resistance of Salmonella enterica serovar Typhimurium. *Molecular Microbiology*, 85(6),1179–1193.

39. Keren, I. et al. (2013). Killing by Bactericidal Antibiotics Does Not Depend on Reactive Oxygen Species. *Science*, 339(6124),1213–1216.

40. Kita, K., Konishi, K. and Anraku, Y. (1984). Terminal oxidases of *Escherichia coli* aerobic respiratory chain. I. Purification and properties of cytochrome b562-o complex from cells in the early exponential phase of aerobic growth. *The journal of biological chemistry*, 259(5), 3368-3374.

41. Kita, K., Konishi, K. and Anraku, Y. (1984). Terminal oxidases of *Escherichia coli* aerobic respiratory chain. II. Purification and properties of cytochrome b558-d complex from cells grown with limited oxygen and evidence of branched electron-carrying systems. *The Journal of biological chemistry*, 259(5), 3375–3381.

42. Kohanski, M.A., Dwyer, D.J. and Collins, J.J. (2010). How antibiotics kill bacteria: from targets to networks. *Nature Reviews Microbiology*, 8(6),423–435.

43. Kohanski, M.A. et al. (2007). A Common Mechanism of Cellular Death Induced by Bactericidal Antibiotics. *Cell*, 130(5),797–810.

44. Lamont, J.T. and Leffler, D.A. (2015). *Clostridium difficle* infection. *N Eng J Med*, 372(16), 1539-1548.

45. Laupland, K.B. and Pitout, J.D. (2008). Extended- spectrum beta lactamase producing Enterobacteriaceae: an emerging public health concern. *Lancet infect dis,* 2008(8), 159-166.

46. Leclercq, R. (2002). Mechanisms of Resistance to Macrolides and Lincosamides: Nature of the Resistance Elements and Their Clinical Implications. *Clinical Infectious Diseases*, 34(4), 482–492.

47. Lee, H., Popodi, E., Tang, H. and Foster, P.L. (2012). Rate and molecular spectrum of spontaneous mutations in the bacterium *Escherichia coli* as determined by whole-genome sequencing. *Proc Natl Acad Sci U S A*, 109(41),e2774-83.

48. Liu, Y. and Imlay, J.A. (2013). Cell Death from Antibiotics Without the Involvement of Reactive Oxygen Species. *Science*, 339(6124),1210–1213.

49. Lobritz, M.A. et al. (2015). Antibiotic efficacy is linked to bacterial cellular respiration. *Proceedings of the National Academy of Sciences*, 112(27),8173–8180.

50. Makarenkov, V., Kevorkov, D. and Legendre, P. (2006). Phylogenetic network construction approaches. *Applied mycology and biotechnology*,2006(6),70-71.

51. Marshall, B.M. and Levy, S.B. (2011). Food animals and antimicrobials: impacts on human health. *Clin Microbiol rev*, 24(4), 718-733.

52. Mason, M.G. et al. (2009). Cytochrome bd confers nitric oxide resistance to *Escherichia coli*. *Nature chemical biology*, 5(2), 94-96.

53. McCollister, B. D., Hoffman, M., Husain, M. and Vázquez-Torres, A. (2011). Nitric oxide protects bacteria from aminoglycosides by blocking the energy-

dependent phases of drug uptake. *Antimicrobial agents and chemotherapy*, 55(5), 2189–2196.

54. Micheal, C.A., Dominey-Howes, D. and Labbate, M. (2014). The antimicrobial resistance crisis: causes, consequences and management. *Front public health*, 2014(2),145.

55. Mulani, M. S., Kamble, E. E., Kumkar, S. N., Tawre, M. S. and Pardesi, K. R. (2019). Emerging Strategies to Combat ESKAPE Pathogens in the Era of Antimicrobial Resistance: A Review. *Frontiers in microbiology*, 10(539), 1-24.

56. Murray, I. A. and Shaw, W. V. (1997). O-Acetyltransferases for chloramphenicol and other natural products. *Antimicrobial agents and chemotherapy*, 41(1), 1–6.

57. Pandey, N. and Cascella, M. (2020). *Beta Lactam Antibiotics*. Statpearls. Available from https://www.ncbi.nlm.nih.gov/books/NBK545311/#article-18243.s8. [Accessed 20 May 2020].

58. Piddock, L.J. (2012). The crisis of no new antibiotics- what is the way forward? *Lancet infect dis,*12(3),249-253.

59. Poock, S.R., Leach, E.M., Moir, J.W.B., Cole, J.A. and Richardson, D.J. (2002). Respiratory Detoxification of Nitric Oxide by the Cytochrome c Nitrite Reductase of *Escherichia coli*. *The journal of biological chemistry*, 277(26), 23664-23669.

60. Poole, R.K., Williams, H.D., Downie, J.A. and Gibson, F. (1989). Mutations affecting the cytochrome d- containing oxidase complex of *Escherichia coli* k12: Identification and mapping of a fourth locus, CydD. *Journal of general microbiology*, 135(7), 1865-1874.

61. Portnoy, V.A., Herrgård, M.J. and Palsson, B.Ø. (2008). Aerobic fermentation of D-glucose by an evolved cytochrome oxidase- deficient *Escherichia coli* strain. *Applied and environmental microbiology*, 74(24),7561-7569.

62. Pullan, S.T. et al. (2007). Nitric Oxide in Chemostat-Cultured *Escherichia coli* Is Sensed by Fnr and Other Global Regulators: Unaltered Methionine Biosynthesis Indicates Lack of S Nitrosation. *Journal of Bacteriology*, 189(5),1845-1855.

63. Puustinen, A., Finel, M., Haltia, T., Gennis, R.B. and Wikström, M. (1991). Properties of the two terminal oxidases of *Escherichia coli*. *Biochemistry*, 30(16),3936–3942.

64. Ribeiro, C. (2018). *Nitric oxide tolerance and antimicrobial susceptibility in Escherichia coli clinical isolates*. School of Biosciences. Canterbury: University of Kent. PhD thesis.

65. Renggli, S. et al. (2013). Role of Autofluorescence in Flow Cytometric Analysis of *Escherichia coli* Treated with Bactericidal Antibiotics. *Journal of Bacteriology*,195,4067–4073.

66. Robinson, J.L., Adolfsen, K.J. and Brynilden, M.P. (2014). Deciphering nitric oxide stress in bacteria with quantitative modelling. *Curr Opin Microbiol*, 2014(19), 16-24.

67. Rőszer, T. (2012). *The Biology of Subcellular Nitric Oxide.* [Online]. Dordrecht: Springer Netherlands.

68. Safarian, S. et al. (2019). Active site rearrangement and structural divergence in prokaryotic respiratory oxidases. *Science*, 6461(366), 100-104.

69. Sarkar, S. et al. (2016). Comprehensive analysis of type 1 fimbriae regulation in fimB- null strains from the multidrug resistant *Escherichia coli* ST131 clone. *Molecular microbiology*, 101(6),1069-1087.

70. Sengupta, S., Chattopadhyay, M.K. and Grossart, H.P. (2013). The multifaceted roles of antibiotics and antibiotic resistance in nature. *Front microbiol*, 12(4),47.

71. Shepherd, M. et al. (2016). The cytochrome bd-I respiratory oxidase augments survival of multidrug-resistant *Escherichia coli* during infection. *Scientific Reports*, 6(35285),1-10.

72. Singer, A.C., Shaw, H., Rhodes, V. and Hart, A. (2016). Review of antimicrobial resistance in the environment and its relevance to environmental regulators. *Front Microbiol*, 1(7),1728.

73. Soares, G. M., Figueiredo, L. C., Faveri, M., Cortelli, S. C., Duarte, P. M. and Feres, M. (2012). Mechanisms of action of systemic antibiotics used in periodontal treatment and mechanisms of bacterial resistance to these drugs. *Journal of applied oral science*, 20(3), 295–309.

74. Spellberg, B. and Gilbert, D.N. (2014). The future of antibiotics and resistance: a tribute to a career of leadership by John Bartlett. *Clin infect dis*, 59(2),S71-75.

75. Spellberg, B., Srinivasan, A. and Chambers, H.F. (2016). New societal approaches to empowering antibiotic stewardship. *Jama*, 315(12),1229-1230.

76. Te Winkel, J. D., Gray, D. A., Seistrup, K. H., Hamoen, L. W. and Strahl, H. (2016). Analysis of Antimicrobial-Triggered Membrane Depolarization Using Voltage Sensitive Dyes. *Frontiers in cell and developmental biology*, 4(29),1-10.

77. Theβeling, A. et al. (2019). Homologous bd-oxidases share the same architecture but differ in mechanism. *Nat commun*, 2019(10), 5138.

78. Tipper, D. J. and Strominger, J. L. (1965). Mechanism of action of penicillins: a proposal based on their structural similarity to acyl-D-alanyl-D-alanine. *Proceedings of the National Academy of Sciences of the United States of America*, 54(4), 1133–1141.

79. Totsika, M. et al. (2011). Insights into a Multidrug Resistant *Escherichia coli* Pathogen of the Globally Disseminated ST131 Lineage: Genome Analysis and Virulence Mechanisms. *PLOS one*, 6(10),e26578.

80. Van Acker, H. and Coenye, T. (2017). The Role of Reactive Oxygen Species in Antibiotic-Mediated Killing of Bacteria. *Trends in Microbiology*, 25(6),456–466.

81. Van den Berg, W.A.M., Hagen, W.R. and Van Dongen, W.M.A.M. (2000). The hybrid-cluster protein ('prismane protein') from *Escherichia coli. European Journal of Biochemistry*, 267(3),666–676.

82. Wang, J. et al. (2016). The roles of the hybrid cluster protein, Hcp and its reductase, Hcr, in high affinity nitric oxide reduction that protects anaerobic cultures of *Escherichia coli* against nitrosative stress. *Mol Microbiol*, 2016(100),877–892.

83. Wang, W. H., Lu, J. X., Yao, P., Xie, Y. and Huang, Z. X. (2003). The distinct heme coordination environments and heme-binding stabilities of His39Ser and His39Cys mutants of cytochrome b5. *Protein engineering*, 16(12), 1047–1054.

84. Woody, A. (2019). *Investigating the effects of nitric oxide upon antibiotic susceptibility in pathogenic Escherichia coli*. School of Biosciences. Canterbury: University of Kent. MSc Thesis.

85. Wu, M., Maier, E., Benz, R. and Hancock, R.E.W. (1999). Mechanism of Interaction of Different Classes of Cationic Antimicrobial Peptides with Planer Bilayers and with the Cytoplasmic Membrane of *Escherichia coli*. *Biochemistry*, 1999(38), 7235-7242.

86. Zhao, X. and Drlica, K. (2014). Reactive oxygen species and the bacterial response to lethal stress. *Current Opinion in Microbiology*, 21,1–6.

Appendix

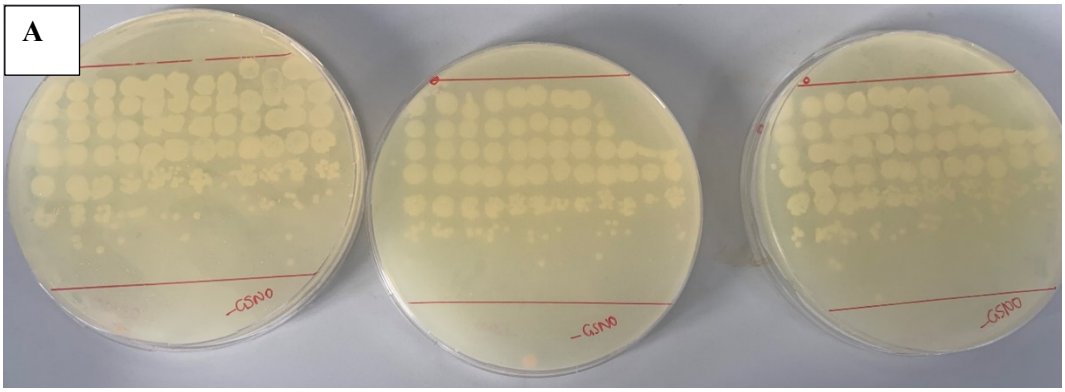
A
-GSNO
-GSNO
-GSNO

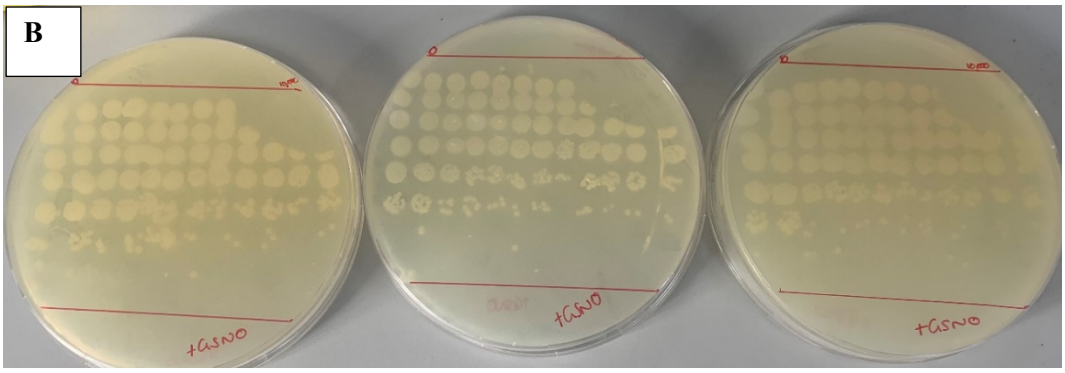
B
+GSNO
+GSNO
+GSNO

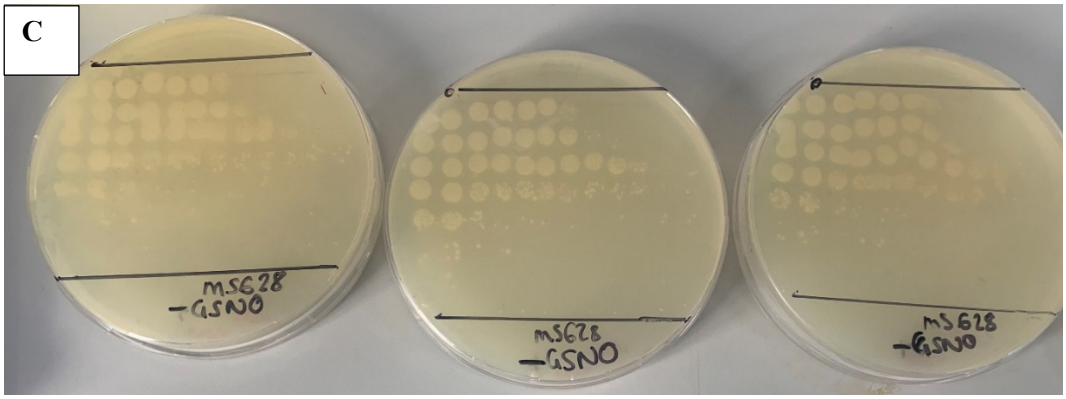
C
MS628
-GSNO
MS628
-GSNO
MS628
-GSNO

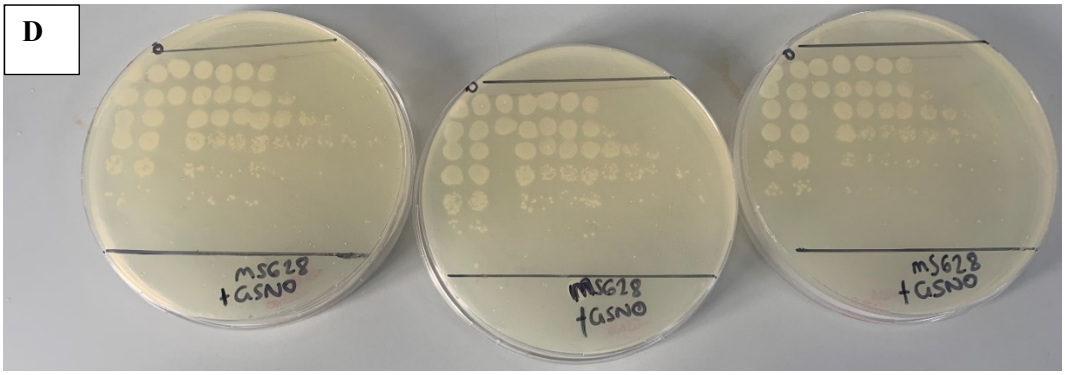
D
MS628
+GSNO
MS628
+GSNO
MS628
+GSNO

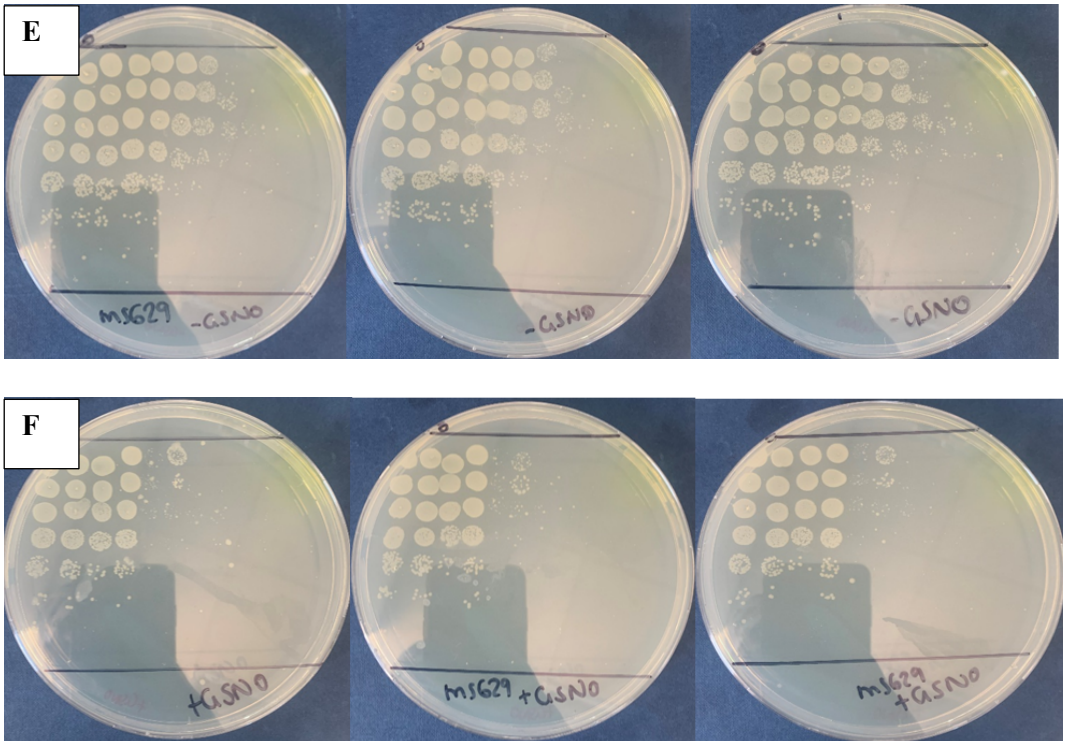

Figure A-Viability assay plates. From colony counts, CFU/ml counts were performed . Technical repeats were conducted from a biological repeat shown above from MS10 (WT) in the absence (A) and presence of (B) GSNO; MS628 (*bd*-I only) in the absence (C) and presence of (D) GSNO; MS629 (*bo´* only) in the absence (E) and presence (F) of GSNO

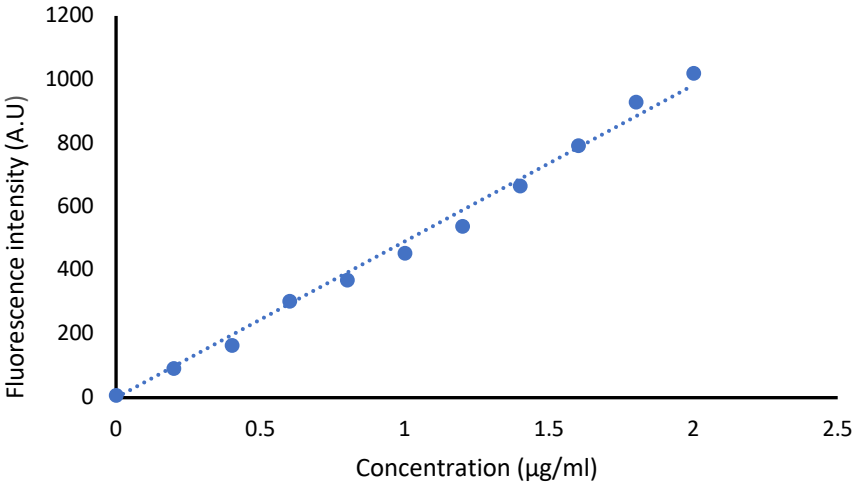

Figure B -Standard curve of $DISC_3(5)$. The standard curve was obtained by making a series of concentrations (0-2µM) in 0.2 µM steps using HEPES buffer as the diluent at an excitation wavelength of 662 nm and emission of 670 nm with a gain of 1000 using BMG labtech SPECTROstar fluorescence settings.

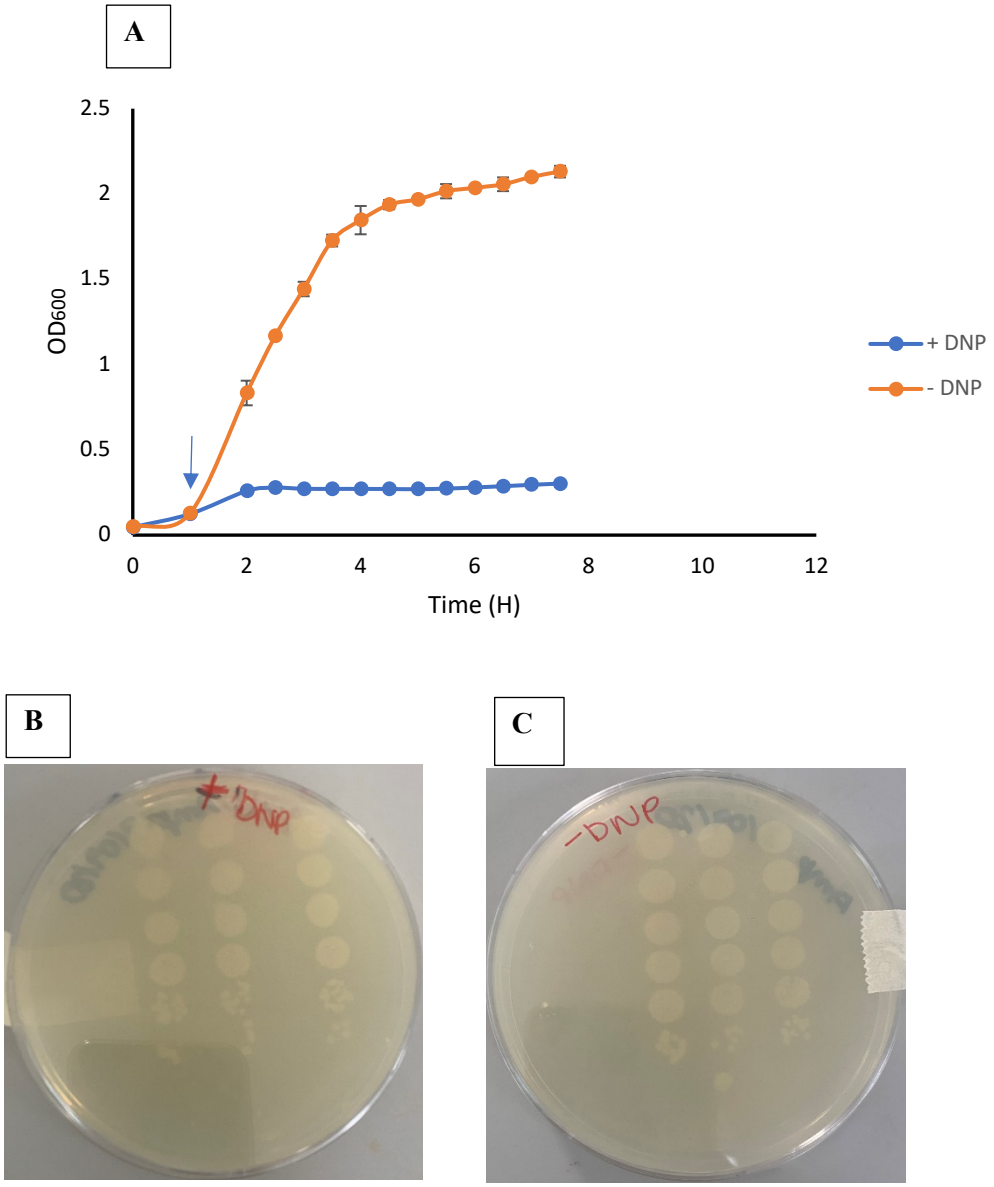

Figure C- Sensitivity of Wild-type *E. coli* strain to 2,4- DNP. (A) Cultures were exposed to M9 minimal media at 37°C in 250 ml conical flask at 180 rpm for aerobic growth. 1 mM of 2,4- DNP was added when the cells reached an OD_{600} of roughly 0.125, this is indicated by the blue arrows. The averages of the three biological repeats represents the data points. The standard deviation is represented by the error bars. Spotting of *E. coli* strain after 24 h exposure with (B) and without (C) 2,4- DNP